ATTACHMENT (6)

UNIT 1 PRESSURIZER HEATER SLEEVE AS-LEFT J-GROOVE WELD FLAW EVALUATION FOR IDTB REPAIR – NON-PROPRIETARY

Calvert Cliffs Nuclear Power Plant, LLC
May 11, 2011

AREVA

CALCULATION SUMMARY SHEET (CSS)

Document No. 32 - 9156231 - 000 Safety Related: ☒ Yes ☐ No

Title CCNPP-1 PZR Heater Sleeve As-Left J-Groove Weld Flaw Evaluation for IDTB Repair

PURPOSE AND SUMMARY OF RESULTS:

Purpose

The purpose of the present analysis is to determine from a fracture mechanics viewpoint the suitability of leaving degraded J-groove weld material in the Calvert Cliffs Unit 1 pressurizer (PZR) vessel head following the repair of a heater sleeve by the ID temper bead weld (IDTB) procedure. It is postulated that a small flaw in the head would combine with a large stress corrosion crack in the weld and cladding to form a radial corner flaw that would propagate into the low alloy steel head by fatigue crack growth under cyclic loading conditions.

This document provides a non-propriety version of AREVA NP INC document 32-9116467-003.

Summary of Results

Based on a combination of linear-elastic and elastic-plastic fracture mechanics (LEFM and EPFM) analysis of a postulated remaining flaw in the original Alloy 82/182 J-groove weld and cladding material, the Calvert Cliffs Unit 1 PZR lower head is considered to be acceptable for at least { } years of operation from the time the postulated flaw formed in the low alloy steel PZR lower head. The controlling loading condition was determined to be the insurge transient Insurge1, for which it was shown that with safety factors of 3 on primary loads and 1.5 on secondary loads that the applied tearing modulus (9.36 for uphill side, and 7.046 for downhill side) was still less than the tearing modulus of the low alloy steel head material (9.38 for uphill side, and 45.736 for downhill side).

[redacted]

THE FOLLOWING COMPUTER CODES HAVE BEEN USED IN THIS DOCUMENT:		THE DOCUMENT CONTAINS ASSUMPTIONS THAT SHALL BE VERIFIED PRIOR TO USE
CODE/VERSION/REV	CODE/VERSION/REV	☐ YES
ANSYS/12/0		☒ NO

AREVA

0402-01-F01 (20697) (Rev. 015, 10/18/2010)
Document No. 32-9156231-000

CCNPP-1 PZR Heater Sleeve As-Left J-Groove Weld Flaw Evaluation for IDTB Repair

Review Method: ☒ Design Review (Detailed Check)
☐ Alternate Calculation

Signature Block

Name and Title (printed or typed)	Signature	P/R/A and LP/LR	Date	Pages/Sections Prepared/Reviewed/Approved
Pei-Yuan Cheng Engineer III	Pei-Yuan Cheng	P	3/11/11	All
Heqin Xu Principal Engineer	[signature]	R	3/11/11	All
T. M. Wiger Unit Manager	[signature]	A	3/11/11	All

Note: P/R/A designates Preparer (P), Reviewer (R), Approver (A);
LP/LR designates Lead Preparer (LP), Lead Reviewer (LR)

Project Manager Approval of Customer References (N/A if not applicable)

Name (printed or typed)	Title (printed or typed)	Signature	Date
N/A			

Mentoring Information (not required per 0402-01)

Name (printed or typed)	Title (printed or typed)	Mentor to: (P/R)	Signature	Date
N/R				
N/R				

Record of Revision

Revision No.	Date	Pages/Sections/ Paragraphs Changed	Brief Description / Change Authorization
000	03/2011	All	Original release

Table of Contents

Page

Table of Contents
(continued)

List of Tables

List of Figures

1.0 INTRODUCTION

Small diameter Alloy 600 nozzles, such as Pressurizer (PZR) heater sleeves, have experienced leaks as a result of primary water stress corrosion cracking (PWSCC) at Calvert Cliffs Unit 1. AREVA will perform the modification and associated engineering analyses required for several PZR heater penetrations at Calvert Cliffs Unit 1 (CCNPP-1) as repair or mitigation [1]. AREVA will utilize the half-nozzle approach to modify the PZR heater sleeves. As shown in Figure 1-1, a portion of the existing heater sleeve will be removed, the outer portion of the penetration will be bored out larger than the original diameter to accept the replacement sleeve and accommodate the inside diameter temper bead (IDTB) weld head. The new stainless steel lower sleeve will be inserted into the penetration. The ambient temperature temper bead welding technique, using the gas tungsten arc welding (GTAW) process with stainless steel filler metal, will attach the new sleeve to the bore ID, establishing a new pressure boundary weld. The IDTB weld is disassociated from the original heater sleeve. The repair is more fully described by the design specification [1] and the design drawing [2]. Although the remnant J-groove weld would no longer be associated with the primary pressure boundary, a defect in the weld could grow into the low alloy steel PZR lower head and thereby impact the structural integrity of the remaining pressure boundary. Since a potential, or even detected, flaw in the J-groove weld can not be sized by currently available non-destructive examination techniques, it is assumed that the "as-left" condition of the remnant J-groove weld includes degraded or cracked weld material extending through the J-groove weld and the entire cladding thickness in the vicinity of the nozzle penetration.

It is postulated that a radial crack in the Alloy 82/182 weld metal would propagate by PWSCC, through the weld and cladding, to the interface between the cladding and the head material, where it is fully expected that such a crack would then blunt, or arrest, as discussed in Reference [3] for interfaces with low alloy steels. Although primary water stress corrosion cracking would not extend into the head, it is further postulated that a small fatigue initiated flaw forms in the low alloy steel head and combines with the stress corrosion crack in the weld and cladding to form a large radial flaw that would propagate into the head by fatigue crack growth under cyclic loading conditions. Linear-elastic (LEFM) and elastic-plastic (EPFM) fracture mechanics procedures are utilized to evaluate this worst case flaw.

Key features of the fracture mechanics analysis are:

- This analysis applies specifically to the PZR heater sleeve penetrations in the Calvert Cliff Unit 1 PZR lower head. A J-integral resistance curve is developed based on estimates of the Charpy V-notch upper-shelf energy for the PZR head.
- Flaw growth is calculated for a 40-year period of operation. However, the remaining life of the component will be estimated based on the flaw evaluation procedures performed in this document.
- Flaw acceptance is based on the available fracture toughness and ductile tearing resistance of the PZR lower head material considering the safety factors listed in Table 1-1.

Table 1-1: Safety Factors for Flaw Acceptance

Linear-Elastic Fracture Mechanics			
Operating Condition	Evaluation Method	Fracture Toughness / K_I	
Normal/Upset	K_{Ia} fracture toughness	$\sqrt{10} = 3.16$	
Emergency/Faulted	K_{Ic} fracture toughness	$\sqrt{2} = 1.41$	
Elastic-Plastic Fracture Mechanics			
Operating Condition	Evaluation Method	Primary	Secondary
Normal/Upset	J/T based flaw stability	3.0	1.5
Normal/Upset	$J_{0.1}$ limited flaw extension	1.5	1.0
Emergency/Faulted	J/T based flaw stability	1.5	1.0
Emergency/Faulted	$J_{0.1}$ limited flaw extension	1.5	1.0

Figure 1-1: ID Temper Bead Weld Repair

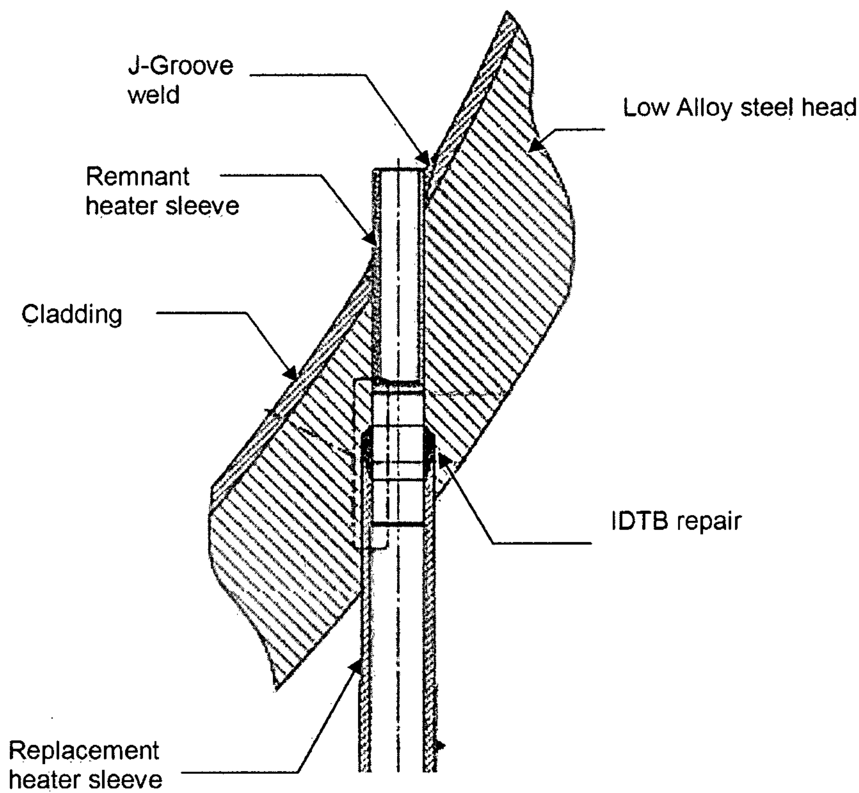

2.0 ANALYTICAL METHODOLOGY

A radial flaw at the inside corner of non-radial head penetration is evaluated based on a combination of linear-elastic fracture mechanics (LEFM) and elastic-plastic fracture mechanics (EPFM), as outlined below.

1. Postulate a radial flaw in the J-groove weld, extending from the inside corner of the penetration to the interface between the cladding and low alloy steel head, as shown in Figure 2-1 and Figure 2-2 for both the downhill and uphill sides of the heater sleeve penetration.

2. Develop two three-dimensional finite element crack models, one for the uphill side crack, and the other for the downhill side crack, of the PZR heater sleeve penetration in the vicinity of the outermost nozzle penetration. Crack tip elements are modeled in the cladding and along the interface between the cladding and the low alloy steel base metal. This crack model will be used to obtain stress intensity factors at various positions along the crack front for combined stresses due to the welding processes and transient loading conditions.

3. Develop a mapping procedure to transfer stresses from uncracked finite element stress analysis models (for residual and operational stresses) to the crack face of the crack model. This will enable stress intensity factors to be calculated for arbitrary stress distributions over the crack face utilizing the principle of superposition.

4. Calculate fatigue crack growth for cyclic loading conditions using combined residual and operational stresses from pressure and thermal loads. It is noted that the only effect of residual stress on fatigue crack growth is in the calculation of the R ratio, or K_{min}/K_{max}, which is the ratio of the minimum and maximum stress intensity factors for a pair of stress states. Starting from the stress intensity factor calculated by the finite element crack model for the initial flaw size, stress intensity factors are updated for each increment of crack growth by the square root of the ratio of the flaw sizes over the increment.

5. Utilize the screening criteria of ASME Code Section XI, Appendix C to determine the failure mode and appropriate method of analysis (LEFM or EPFM) for flaws in ferritic materials, considering the applied stress, temperature, and material toughness. For LEFM flaw evaluations, compare the stress intensity factor at the final flaw size to the available fracture toughness, with appropriate safety factors, as discussed in Section 2.3. When the material is more ductile and EPFM is the appropriate analysis method, evaluate flaw stability and crack driving force as described in Section 2.4.

Figure 2-1: Downhill Side Postulated Radial Flaw

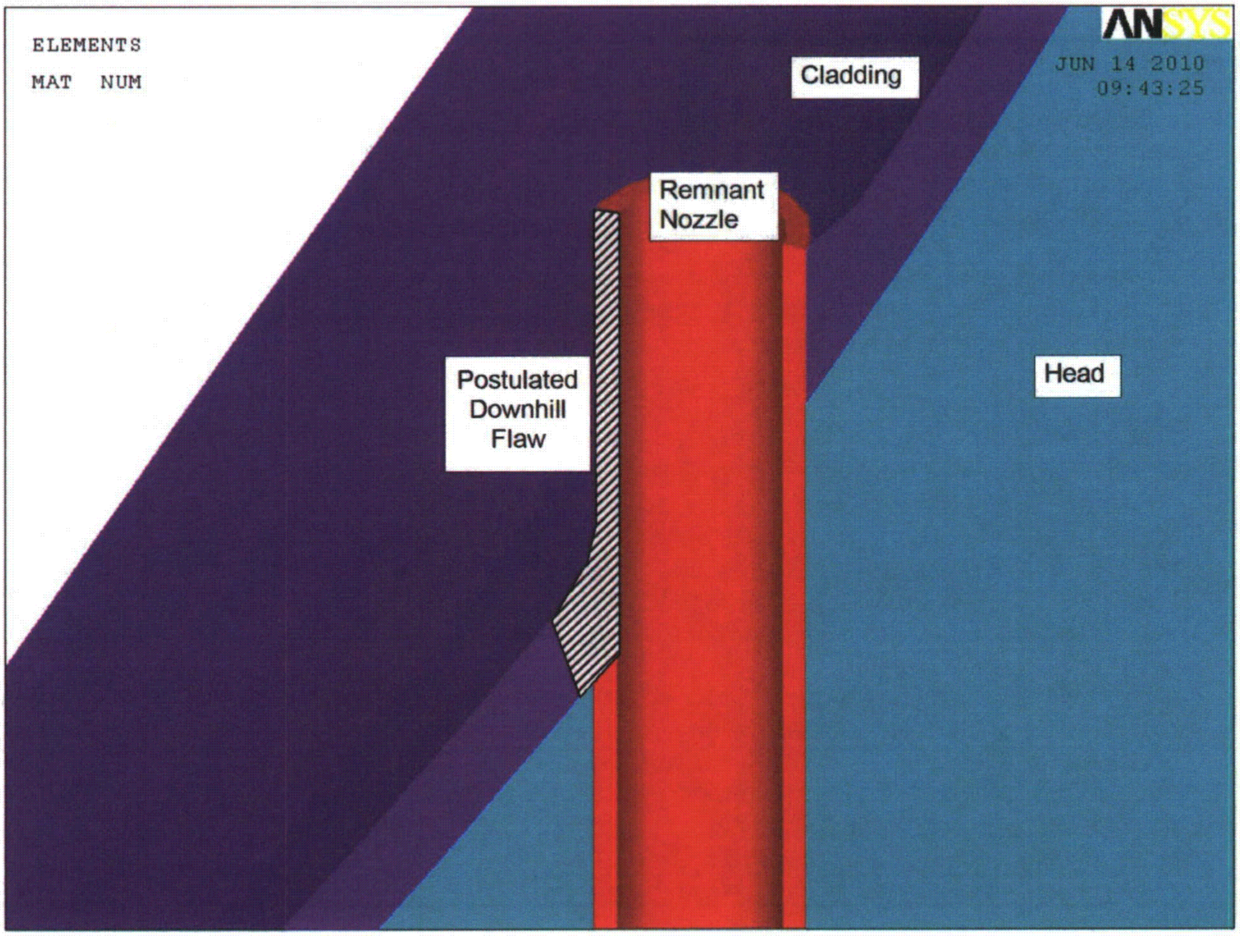

Figure 2-2: Uphill Side Postulated Radial Flaw

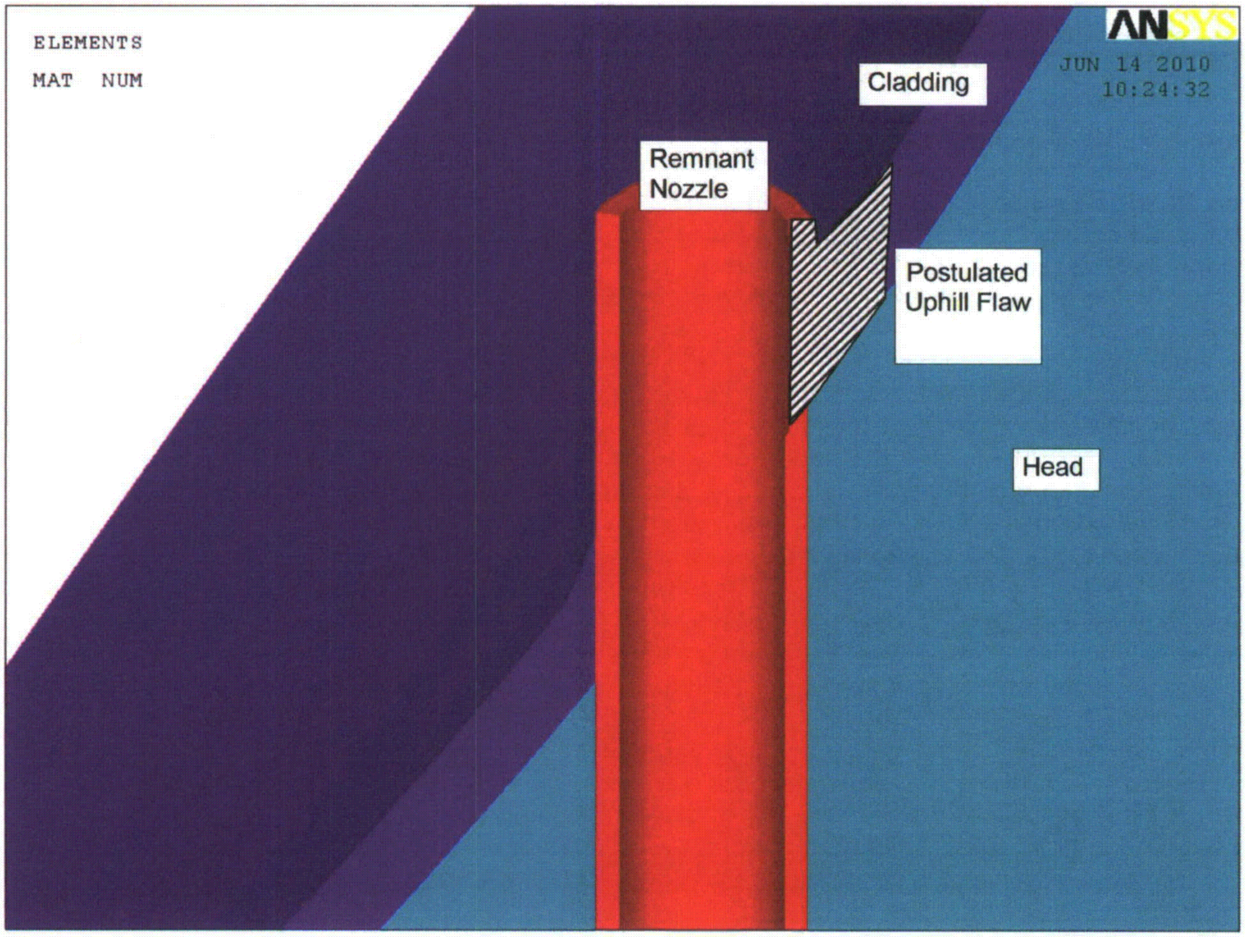

2.1 Stress Intensity Factor Solution

Stress intensity factors for corner flaws at a non-radial nozzle penetration are best determined by finite element analysis using three-dimensional models with crack tip elements along the crack front. Although loads can be applied to finite element crack models like any other structural model, the crack models were developed to serve as a flaw evaluation tool that could accept stresses from separate stress analyses. This strategy makes it possible, for example, to obtain pressure and thermal stresses from an independent thermal/structural analysis and then transfer these stresses to a crack model for flaw evaluations. Using the principle of superposition common to fracture mechanics analysis, the only stresses that need be considered for these flaw evaluations are the stresses on the crack face. A mapping procedure is developed to transfer stresses from a separate stress analysis to the crack face of the crack models.

2.1.1 Finite Element Crack Models

Two three-dimensional finite element models are developed for the PZR lower head in the vicinity of the outermost heat sleeve penetration, by modeling a portion of the head, cladding, and the remnant nozzle with the ANSYS finite element computer program [4]. Since stresses increase with penetration angle, it is conservative to base the model on the outermost nozzle penetration. Details of the finite element crack models are presented in Appendix C.

The three-dimensional finite element models are first constructed to represent an unflawed non-radial nozzle penetration in the PZR lower head using the ANSYS SOLID186 20-node structural element. Elements along the crack front are then replaced by a sub-model of crack tip elements in the cladding and along the interface between the cladding and the low alloy steel head. These elements consist of 20-node isoparametric elements that are collapsed to form a wedge with the appropriate mid-side nodes shifted to quarter-point locations to simulate a singularity at the crack tip. The final crack models are shown in Figure 2-3 and Figure 2-4 for the downhill and uphill sides of the PZR heater sleeve penetration, respectively. Linear contact elements were used to bond various parts of the model to simplify meshing.

Stress intensity factors are obtained using the DH_K1Kcalc.mac and UH_K1Kcalc.mac files, which contain a set of ANSYS parametric design language instructions which implements similar theory to the ANSYS KCALC routine. The DH_K1Kcalc.mac and UH_K1Kcalc.mac ANSYS command sets files were verified against the ANSYS KCALC routine in Appendix A. SIF values are calculated at each crack tip node position along the crack front, as indicated in Figure 2-3 and Figure 2-4. For both the downhill and uphill sides, Position 1 is located on the cladding surface and the last position is along the remnant nozzle inner surface.

2.1.2 Stress Mapping

Residual and operational stresses, obtained from separate finite element models, are mapped onto the crack face of the finite element crack model shown in Figure 2-3 and Figure 2-4 to calculate the individual contributions to the stress intensity factors. A set of ANSYS parametric design language instructions has been written based on the *MOPER, MAP command to transfer stresses by nodal interpolation from a dissimilar finite element model (e.g., residual stresses and operating stresses) to the crack model.

Figure 2-3: Downhill Side Finite Element Crack Model

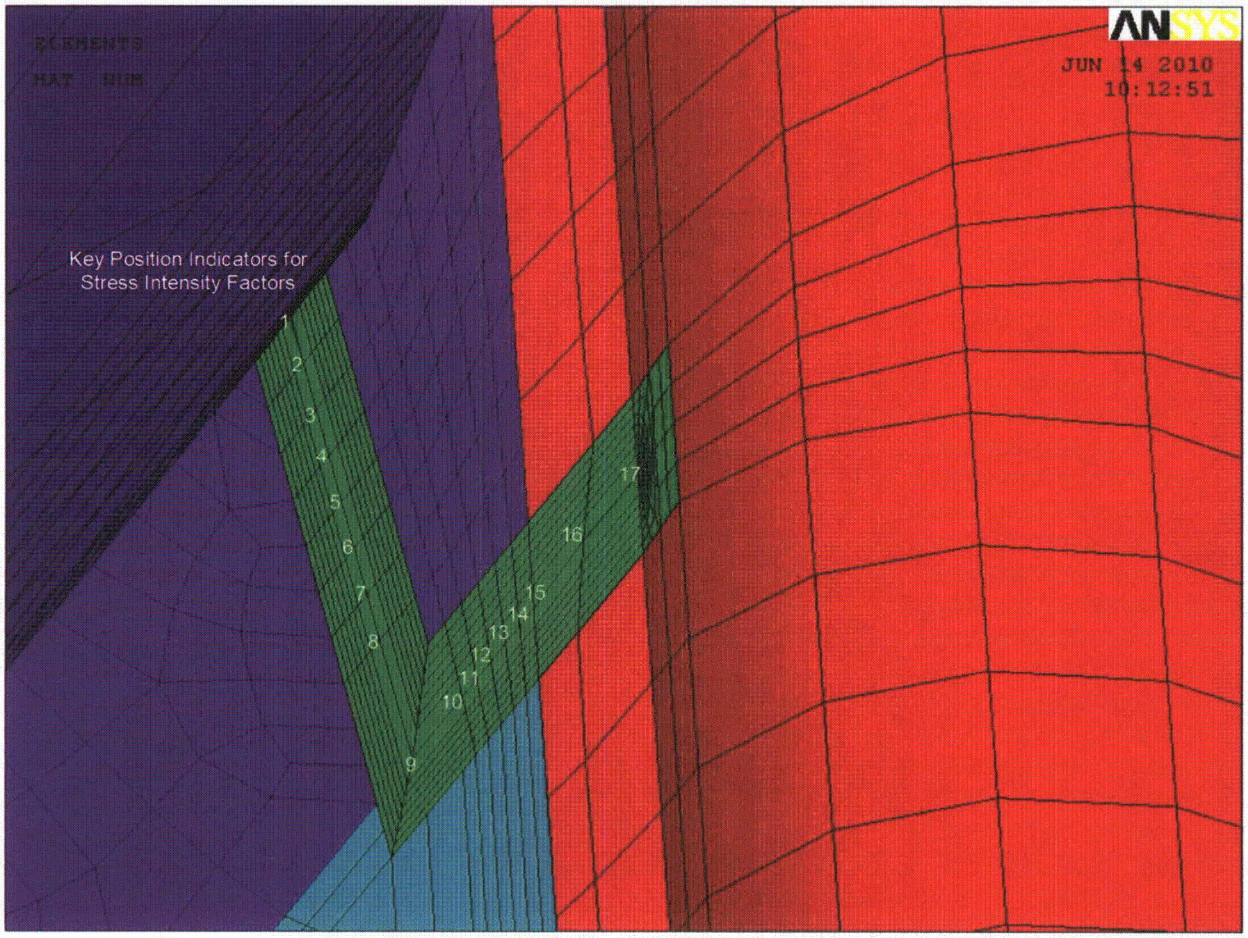

Figure 2-4: Uphill Side Finite Element Crack Model

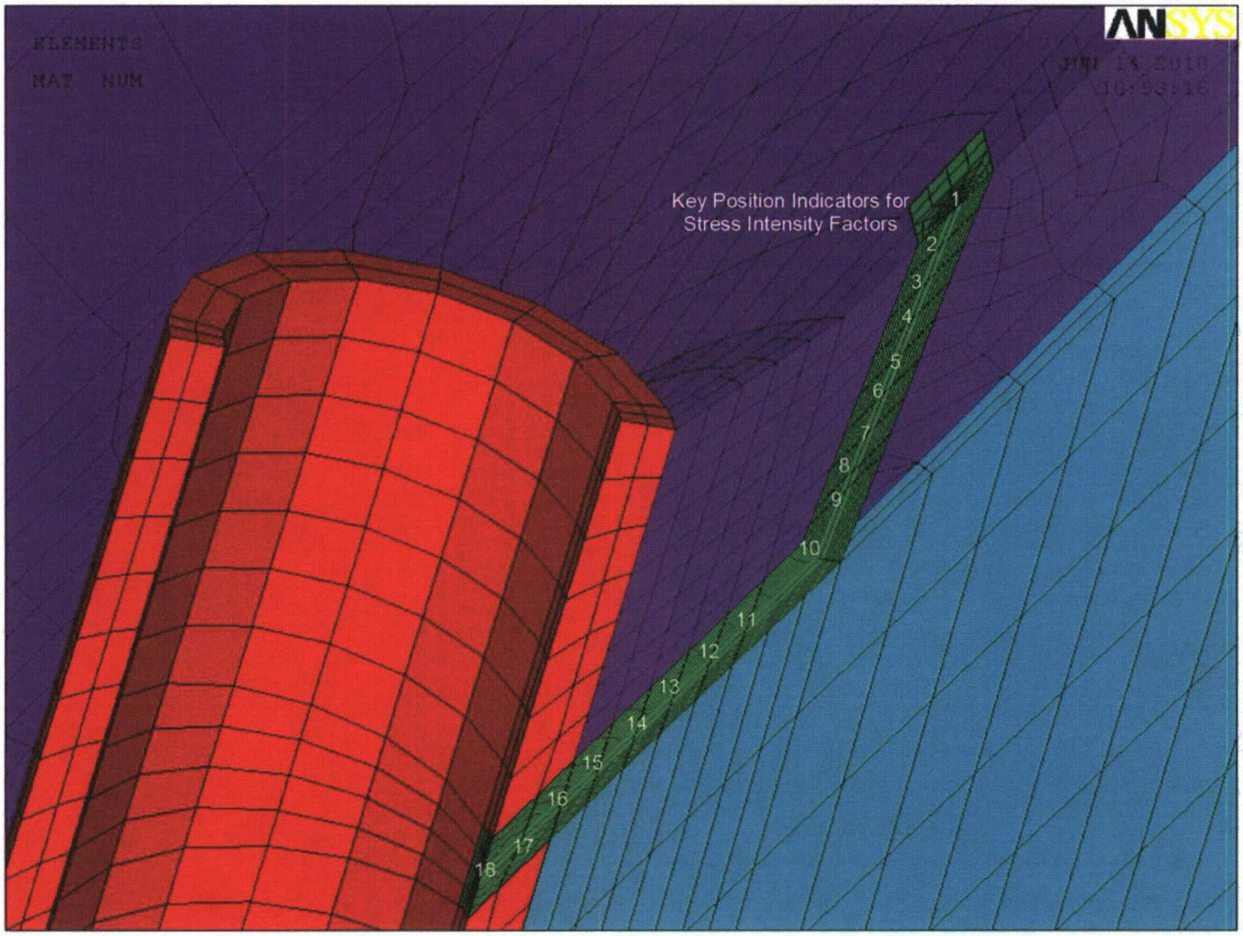

2.2 Crack Growth Considerations

The fundamental expression for the crack tip stress intensity factor is

$$K_I = \sigma\sqrt{\pi a}$$

Since the crack model is developed for a single flaw size, stress intensity factors are updated at each increment of crack growth by the square root of the flaw size; i.e.,

$$K_I(a_{i+1}) = K_I(a)\sqrt{\frac{a_{i+1}}{a_i}},$$

where a = flaw size

i = increment of crack growth.

Since the stress intensity factor is directly proportional to the magnitude of the stress and both residual and operating stresses decrease in the direction of crack growth, this procedure produces conservative estimates of stress intensity factor as the crack extends into the head and stresses diminish over the expanding crack face.

2.2.1 Plastic Zone Correction

The Irwin plasticity correction is used to account for a moderate amount of yielding at the crack tip. For plane strain conditions, this correction is

$$r_y = \frac{1}{6\pi}\left(\frac{K_I(a)}{\sigma_y}\right)^2, \qquad \text{[Ref. [5], Eqn. (2.63)]}$$

where $K_I(a)$ = stress intensity factor based on the actual crack size, a

σ_y = material yield strength.

A stress intensity factor, $K_I(a_e)$, is then calculated for an effective crack size,

$$a_e = a + r_y,$$

based on the same scaling technique utilized for crack growth; i.e.,

$$K_I(a_e) = K_I(a)\sqrt{\frac{a_e}{a}}.$$

2.3 Linear-Elastic Fracture Mechanics

Article IWB-3612 of Section XI [7] requires that the applied stress intensity factor, K_I, at the final flaw size be less than the available fracture toughness at the crack tip temperature, with appropriate safety factors, as outlined below.

Normal and upset conditions: $K_I < K_{Ia} / \sqrt{10}$

Emergency and faulted conditions: $K_I < K_{IC} / \sqrt{2}$

where K_{Ic} is the fracture toughness based on crack initiation.

2.4 Elastic-Plastic Fracture Mechanics

Elastic-plastic fracture mechanics (EPFM) will be used as alternative acceptance criteria when the flaw related failure mechanism is unstable ductile tearing. This type of failure falls between rapid, non-ductile crack extension and plastic collapse. Linear-elastic fracture mechanics (LEFM) would be used to assess the potential for non-ductile failure, whereas limit load analysis may be used to check for plastic collapse.

2.4.1 Screening Criteria

Screening criteria for determining failure modes in ferritic materials may be found in Appendix C of Section XI. Although Appendix C, Article C-4200 [7] contains specific rules for evaluating flaws in Class 1 ferritic piping, its screening criteria may be adapted to other ferritic components, such as the PZR head, as follows:

Let, $K_r' = K_{Iapp} / K_{Ic}$

$S_r' = \sigma_{max} / \sigma_f$

Then the appropriate method of analysis is determined by the following limits:

LEFM Regime:		$K_r' / S_r' \geq 1.8$
EPFM Regime:	$1.8 >$	$K_r' / S_r' \geq 0.2$
Limit Load Regime:	$0.2 >$	K_r' / S_r'

2.4.2 Flaw Stability and Crack Driving Force

Elastic-plastic fracture mechanics analysis will be performed using a J-integral/tearing modulus (J-T) diagram to evaluate flaw stability under ductile tearing, where J is either the applied (J_{app}) or the material (J_{mat}) J-integral, and T is the tearing modulus, defined as $(E/\sigma_f^2)(dJ/da)$. The crack driving force, as measured by J_{app}, is also checked against the J-R curve at a crack extension of 0.1 inch ($J_{0.1}$). Consistent with industry practice for the evaluation of flaws in partial penetration welded nozzles, different safety factors will be utilized for primary and secondary loads. Flaw stability assessments for normal and upset conditions will consider a safety factor of 3 on the stress intensity factor due to primary (pressure) stresses and a safety factor of 1.5 for secondary (residual plus thermal) stresses. The crack driving force will be calculated using safety factors of 1.5 and 1 for primary and secondary stresses, respectively. For EPFM analysis of faulted conditions, safety factors of 1.5 and 1 will be used for flaw stability assessments and 1.5 and 1 for evaluations of crack driving force.

The general methodology for performing an EPFM analysis is outlined below.

Let $E' = E/(1-\nu^2)$

Final flaw depth $= a$

Total applied $K_I = K_{Iapp}$

K_I due to pressure (primary) $= K_{Ip}$ (from Appendix D)

K_I due to residual plus thermal (secondary) $= K_{Is} = K_{Iapp} - K_{Ip}$

Safety factor on primary loads $= SF_p$

Safety factor on secondary loads $= SF_s$

For small scale yielding at the crack tip, a plastic zone correction is used to calculate an effective flaw depth based on

$$a_e = a + [1/(6\pi)] [(K_{Ip} + K_{Is}) / \sigma_y]^2,$$

which is used to update the stress intensity factors based on

$$K'_{Ip} = K_{Ip}\sqrt{\frac{a_e}{a}}$$

and

$$K'_{Is} = K_{Is}\sqrt{\frac{a_e}{a}}.$$

The applied J-integral is then calculated using the relationship

$$J_{app} = (SF_p{*}K'_{Ip} + SF_s{*}K'_{Is})^2/E'.$$

The final parameter needed to construct the J-T diagram is the tearing modulus. The applied tearing modulus, T_{app}, is calculated by numerical differentiation for small increments of crack size (da) about the final crack size (a), according to

$$T_{app} = \frac{E}{\sigma_f^2}\left[\frac{J_{app}(a+da) - J_{app}(a-da)}{2(da)}\right].$$

Using the power law expression for the J-R curve,

$$J_{mat} = C(\Delta a)^m,$$

the material tearing modulus, T_{mat}, can be expressed as

$$T_{mat} = (E/\sigma_f^2)Cm(\Delta a)^{m-1}.$$

Constructing the J-T diagram,

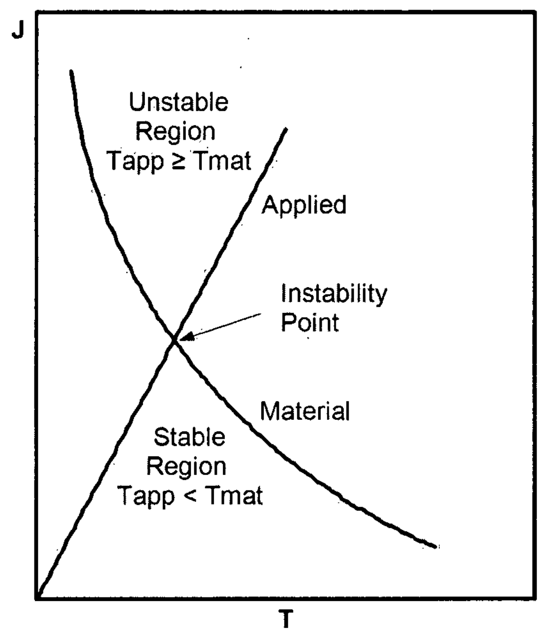

flaw stability is demonstrated at an applied J-integral when the applied tearing modulus is less than the material tearing modulus. Alternately, the applied J-integral is less than the J-integral at the point of instability.

To complete the EPFM analysis, it must be shown that the applied J-integral is less than $J_{0.1}$, demonstrating that the crack driving force falls below the J-R curve at a crack extension of 0.1 inch.

3.0 ASSUMPTIONS

This section discusses assumptions and modeling simplifications applicable to the present evaluation of the CCNPP-1 PZR heater sleeve J-groove weld remnant flaw.

3.1 Unverified Assumptions

This document contains no assumptions that must be verified prior to use on safety-related work.

3.2 Justified Assumptions

It is conservatively assumed that the postulated flaw extends through the entire J-groove weld and adjacent cladding material. The extent of radial flaw size was limited in the radial direction since the residual and operational stresses diminish away from the J-groove weld. The RT_{NDT} is assumed to be 60 °F which is conservative since the RT_{NDT} value for the CCNPP-1 pressurized lower head is 48 °F per reference [6]. The Charpy Upper Shelf Energy value of 70 ft-lbs is assumed. This is conservative since the Charpy Upper Shelf Energy value for the CCNPP-1 pressurized lower head is 85 ft-lbs per reference [6].

3.3 Modeling Simplifications

The following modeling simplifications were used

1. The finite element model with crack tip elements does not include the ID temper bead repair weld. This is deemed to be an appropriate modeling simplification since the IDTB material does not have any effects to the as-left J-groove weld analysis.

2. Since the J-groove weld partially penetrates the cladding and both materials have similar properties, the J-groove weld boundary is not specifically included in the finite element model with crack tip elements. This is deemed to be an appropriate modeling simplification and will not have any impact on the results.

4.0 DESIGN INPUTS

This section provides basic input data needed to perform a fatigue crack growth analysis and flaw evaluation of the final flaw size.

4.1 Materials

4.1.1 Mechanical and Properties

Table 4-1 and Table 4-2 list the temperature dependent values of modulus of elasticity (E) and Poisson's ratio (ν). These properties are obtained from Reference [9]. Yield, ultimate, and flow strengths for the low alloy steel head are also provided in Table 4-1, where the flow stress is the average of the yield and ultimate strengths.

Component	Material
PZR bottom head	SA-533 Grade B Class 1 [1]
Cladding	Ni-Cr-Fe (use Alloy 600) [1]
J-groove weld filler	Alloy 82/182 (use Alloy 600) [1]
Existing lower level heater sleeve	SB-166, Alloy 600 [1]

Table 4-1: Material Properties for Low Alloy Steel PZR Head

Component	Head				
Material	SA-533 Grade B Class 1				
Temperature	E (10^6 psi)	ν	σ_y (ksi)	σ_u (ksi)	σ_f (ksi)
70	27.90	0.3	50.00	80.0	65.00
100	27.85	0.3	50.00	80.0	65.00
200	27.70	0.3	47.15	80.0	63.58
300	27.40	0.3	45.25	80.0	62.63
400	27.00	0.3	44.50	80.0	62.25
500	26.40	0.3	43.20	80.0	61.60
600	25.70	0.3	42.00	80.0	61.00
650	25.25	0.3	41.40	80.0	60.70
700	24.80	0.3	40.60	80.0	60.30

Table 4-2: Material Properties for Cladding, Weld Filler, Existing Heater Sleeve

Component	Cladding, Weld Filler, Existing Heater Sleeve	
Material	Use Alloy 600 (SB-166)	
Temperature	E (10^6 psi)	ν
70	31.70	0.3
100	31.52	0.3
200	30.90	0.3
300	30.50	0.3
400	30.00	0.3
500	29.60	0.3
600	29.20	0.3
650	28.90	0.3
700	28.60	0.3

4.1.2 Reference Temperature

Per Reference [6], the RT_{NDT} value for the CCNPP-1 pressurized lower head material is { } °F, an RT_{NDT} value of { } °F is conservatively used in this document.

4.1.3 Fracture Toughness

From Article A-4200 of Section XI [7], the lower bound K_{Ia} fracture toughness for crack arrest can be expressed as

$$K_{Ia} = 26.8 + 12.445 \exp [0.0145 (T - RT_{NDT})],$$

where T is the crack tip temperature, RT_{NDT} is the reference nil-ductility temperature of the material, K_{Ia} is in units of ksi√in, and T and RT_{NDT} are in units of °F. In the present flaw evaluations, K_{Ia} is limited to a maximum value of 200 ksi√in (upper-shelf fracture toughness). Using the above equation with an RT_{NDT} of { } °F, K_{Ia} equals 200 ksi√in at a crack tip temperature of { } °F.

A higher measure of fracture toughness is provided by the K_{Ic} fracture toughness for crack initiation, approximated in Article A-4200 of Section XI [7] by

$$K_{Ic} = 33.2 + 20.734 \exp [0.02 (T - RT_{NDT})].$$

4.1.4 J-integral Resistance Curve

The J-integral resistance (J-R) curve, needed for the EPFM method of analysis, is obtained from the following power law expression for nuclear reactor pressure vessel steels [8],

$$J_R = C(\Delta a)^m,$$

where the coefficient, C, and exponent, m, depend on the Charpy V-notch upper-shelf energy, CVN, and the flow stress, σ_o or σ_f, as shown in Figure 4-1 and Figure 4-2.

Per reference [6] the Charpy V-notch upper-shelf energy for the CCNPP-1 pressurized lower head material is { } ft-lbs. However, Charpy V-notch upper-shelf value of { } ft-lbs is used in this document. For an upper-shelf value of { } ft-lbs, the coefficients of the power law are found to be:

C = { }

m = { }, based on the flow stress of { } ksi at room temperature

Figure 4-1: Correlation of Coefficient, C, of Power Law with Charpy V-Notch Upper Shelf Energy

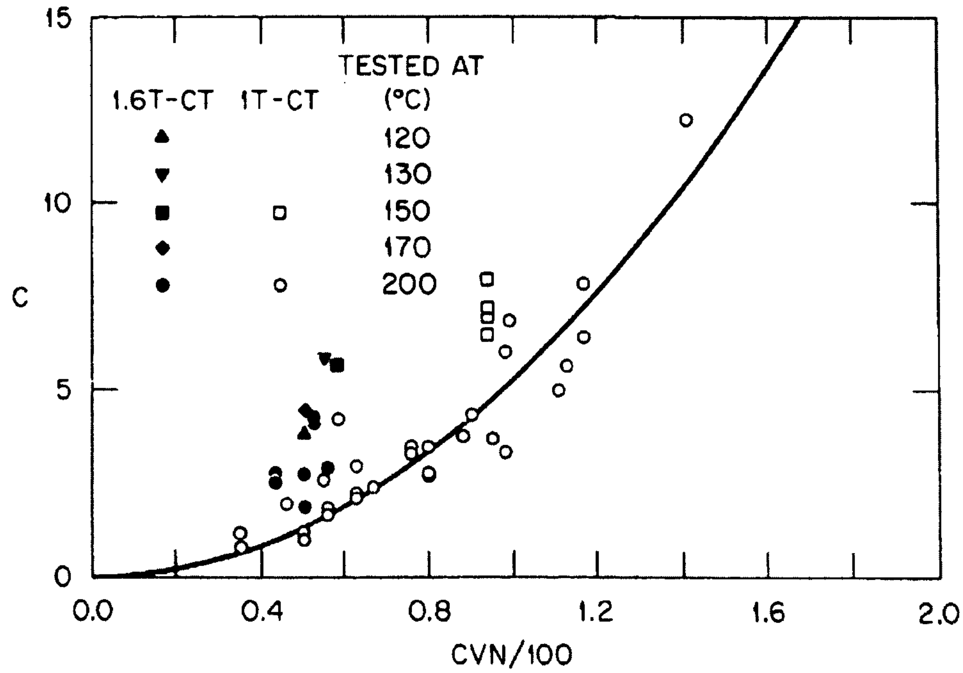

Figure 4-2: Correlation of Exponent, m, of Power Law with Coefficient, C, and Flow Stress, σ_o

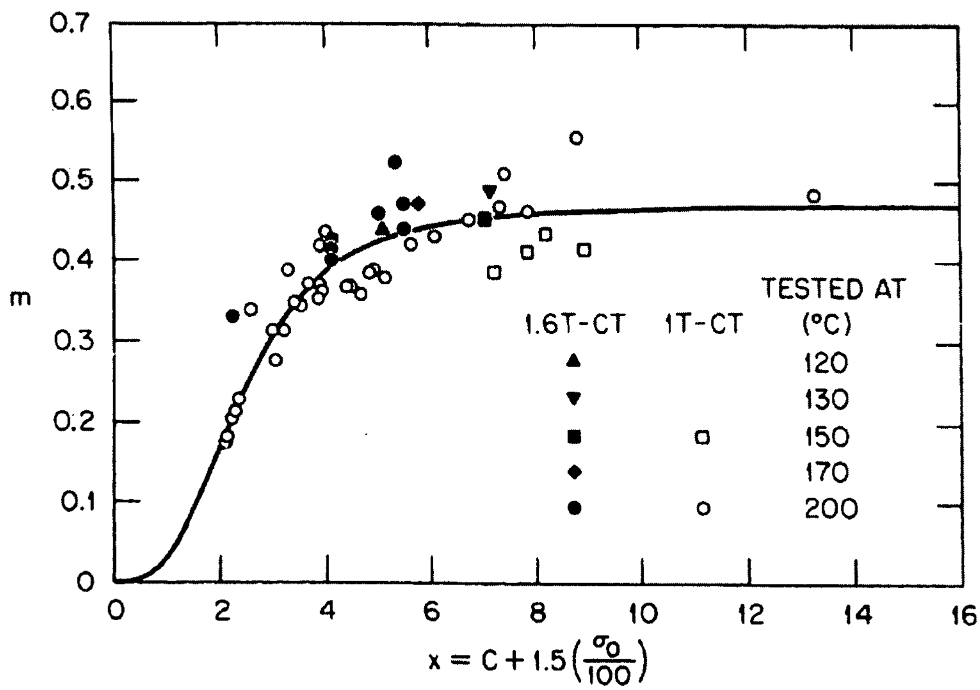

4.1.5 Fatigue Crack Growth Rate

Flaw growth due to cyclic loading is calculated using the fatigue crack growth rate model from Article A-4300 of Section XI [7],

$$\frac{da}{dN} = C_o (\Delta K_I)^n ,$$

where ΔK_I is the stress intensity factor range in ksi√in and da/dN is in inches/cycle. The crack growth rates for a surface flaw will be used for the evaluation of the corner crack since it is assumed that the degraded condition of the J-groove weld and cladding exposes the low alloy steel head material to the primary water environment.

The following equations from Section XI [7] are used to model fatigue crack growth.

$$\Delta KI = KI_{max} - KI_{min}$$
$$R = KI_{min} / KI_{max}$$

$0 \leq R \leq 0.25$: $\Delta K_I < 17.74$,

$$n = 5.95$$
$$C_o = 1.02 \times 10^{-12} \times S$$
$$S = 1.0$$

$\Delta K_I \geq 17.74$,

$$n = 1.95$$
$$C_o = 1.01 \times 10^{-7} \times S$$
$$S = 1.0$$

$0.25 \leq R \leq 0.65$: $\Delta K_I < 17.74 [(3.75R + 0.06) / (26.9R - 5.725)]^{0.25}$,

$$n = 5.95$$
$$C_o = 1.02 \times 10^{-12} \times S$$
$$S = 26.9R - 5.725$$

$\Delta K_I \geq 17.74 [(3.75R + 0.06) / (26.9R - 5.725)]^{0.25}$,

$$n = 1.95$$
$$C_o = 1.01 \times 10^{-7} \times S$$
$$S = 3.75R + 0.06$$

$0.65 \leq R < 1.0$: $\Delta K_I < 12.04$,

$$n = 5.95$$
$$C_o = 1.02 \times 10^{-12} \times S$$
$$S = 11.76$$

$\Delta K_I \geq 12.04$,

$$n = 1.95$$
$$C_o = 1.01 \times 10^{-7} \times S$$
$$S = 2.5$$

4.2 Basic Geometry

The PZR lower head and heater sleeve penetration are described by the following key dimensions:

Radius to base metal	= { } in. [2]
Head thickness (minimum)	= { } in. [2]
Cladding thickness (nominal)	= { } in. [2]
Penetration bore	= { } in. [2]
Penetration to PZR center	= { } in. [2]
Initial Flaw depth	= { } in { }

Details of the PZR heater sleeve penetration are provided in the description of the finite element crack model in Appendix C.

4.3 Operating Transients

The operating conditions (temperature and pressure) transients for the PZR heater sleeve are summarized in Reference [9]. Table 4-3 lists the heater sleeve operating conditions transients and the number of cycles for 40 years of operation.

Table 4-3: Operating Conditions Transients

Condition	Transient Name	Description	Cycle
Normal	1A	{	}
	1B		
	2A		
	2B		
	PL		
	PU		
Test	Leak Test		
Upset	LL		
Insurges	Insurge1		
	Insurge2		
	Insurge3	}	}

Condition	Transient Name	Description	Cycle
	Insurge4		
	Insurge5		
	Insurge6		
	Insurge7		
	Insurge8		
	Insurge9		
	Insurge10		
	Insurge11		
	Insurge12		
	Insurge13		
	Insurge14		

For fatigue flaw growth calculation, the most limiting transient of 1A and 1B will be considered. Similarly, the most limiting transient of 2A and 2B will be considered.

Since the safety factors on fracture toughness are higher for normal/upset conditions than for emergency/faulted conditions (Table 1-1), it follows that the present flaw evaluations for normal/upset conditions also serve as a bounding analysis for emergency and faulted conditions. No further consideration of the emergency and faulted transients is therefore warranted.

4.4 Applied Stresses

Two sources of applied stress are considered for the present flaw evaluations, residual stresses from welding and stresses that occur during normal operation.

4.4.1 Residual Stresses

Residual stresses are obtained from a three-dimensional elastic-plastic finite element stress analysis performed in Reference [10]. Hoop stresses on the radial plane through the J-groove weld and cladding are then mapped to the three-dimensional finite element crack model described in Section 2.1.1. Hoop stresses are used since these stresses are perpendicular to the crack face and therefore open the crack.

Reference [10] simulated welding of the J-groove partial penetration weld at the outmost heater sleeve penetration, hydrostatic testing, operation at steady state temperature and pressure conditions, return to zero load conditions, welding of the IDTB repair, and a second application of steady state loads.

4.4.2 Operational Stresses

Operational stresses are obtained by linear-elastic stress analysis performed in Reference [11] using three-dimensional finite element analysis. Hoop stresses on a radial plane through the crack are provided by Reference [11] to facilitate the calculation of stress intensity factors along the entire crack front. Stresses are developed for the transients discussed in Section 4.3 using the thermal and structural finite element models [12]. The thermal phase of the solution is driven by wetted surface loads developed from time-dependent bulk fluid temperatures and convective heat transfer (film) coefficients. The structural model is then loaded by internal pressure (surface load) and nodal temperatures (body force loads from the thermal solution) to determine stresses at various times. Stresses are provided for all the transients listed in Table 4-3 and for a design case pressure that was simulated at { } F and { } psig in Reference [11].

The critical time points are selected only after calculating stress intensity factors for each set of stresses output from the stress analysis solution. This process serves to maximize the stress intensity factors used in the fatigue crack growth analysis and the final flaw evaluations.

5.0 CALCULATIONS

Propagation of an initial flaw, postulated in the cladding and along the cladding low alloy steel interface, is calculated to determine the final flaw size after a 40-year service interval. Flaw evaluations are then performed to determine the final flaw size and the remaining life.

5.1 Stress Intensity Factor Calculations

The stress intensity factors were calculated using the three-dimensional finite element analysis method for the postulated flaws in both the uphill and downhill sides of the PZR heater sleeve penetration. SIF values were calculated for every crack tip location at every transient time point provided in Reference [11]. The stresses that contributed to the crack driving force are weld residual stresses, operational stresses, and crack face pressure. The stress intensity factors were summarized in files DH_K1.out and UH_K1.out that are archived in the AREVA NP COLDStor repository, as described in Appendix B. Table 5-1 lists the stress intensity selected for every transient that result in maximum crack growth for both uphill and downhill sides. From the results tabulated in Table 5-1, it is shown that transients 1B and 2B have the highest ΔK for the heatup and cooldown transients. Thus, transients 1A and 2A will not be used for crack growth. However, transients 1A and 2A will be considered during flaw evaluation.

Table 5-1: Listing of Selected Stress Intensity Factors Used for Fatigue Crack Growth

Transient	Uphill Side			Downhill Side		
	Kmax (psi√in)	Kmin (psi√in)	ΔK (psi√in)	Kmax (psi√in)	Kmin (psi√in)	ΔK (psi√in)
1A	17042.0	3835.8	13206.2	15683.7	1135.5	14548.2
1B	17042.4	3060.4	13982.0	15684.6	49.2	15635.4
2A	18344.3	8452.0	9892.3	16828.0	5240.0	11588.0
2B	18203.3	8256.9	9946.4	16104.0	4180.2	11923.8
PL	23685.8	21736.7	1949.1	17162.1	15548.0	1614.1
PU	23965.5	21801.3	2164.2	17420.4	15380.1	2040.3
Leak Test	19200.4	7034.7	12165.7	18534.1	3214.2	15319.9
LLA	24586.0	18691.3	5894.7	16644.9	11986.2	4658.7
Insurge1	62775.1	22122.3	40652.8	46620.1	15942.8	30677.3
Insurge2	43880.4	10956.3	32924.1	27245.5	1918.8	25326.7
Insurge3	57621.9	22122.3	35499.6	42567.2	15887.1	26680.1
Insurge4	41603.4	10956.3	30647.1	25347.3	1918.8	23428.5
Insurge5	40477.4	10932.5	29544.9	24648.5	1901.0	22747.5
Insurge6	39218.3	10956.3	28262.0	23642.2	1918.8	21723.4
Insurge7	51499.3	22122.3	29377.0	37955.4	15869.3	22086.1
Insurge8	37569.2	10956.3	26612.9	22410.5	1918.8	20491.7
Insurge9	36294.4	10956.3	25338.1	21557.7	1918.8	19638.9
Insurge10	47450.7	22016.8	25433.9	34904.9	15942.8	18962.1
Insurge11	45275.0	21915.5	23359.5	33459.1	15869.3	17589.8
Insurge12	30902.1	10956.3	19945.8	17440.0	1918.8	15521.2
Insurge13	33848.6	21716.4	12132.2	24754.4	15829.7	8924.7
Insurge14	21169.6	10956.3	10213.3	9820.6	1918.8	7901.8

5.2 Fatigue Crack Growth

Although it is believed that a PWSCC flaw would be confined to the J-groove weld and cladding, it is postulated that a fatigue flaw would initiate in the low alloy steel head, combine with the PWSCC flaw, and propagate farther into the head under cyclic loads. Fatigue crack growth is calculated from stress intensity factors derived from a finite element crack model using residual stresses from Reference [10] and operational stresses from Reference [11]. The SIF values used for fatigue crack growth are tabulated in Table 5-1.

Figure 5-1 and Figure 5-2 show the crack depth as a function of operating years for both the uphill and downhill sides, respectively. Table 5-2 shows the contribution of crack growth from each transient for both the uphill and the downhill sides. It should be noted that the crack in the uphill side was limited to { } years based on the flaw evaluation results described in Sections 5.3 and 5.5.

Details of the crack growth evaluation are shown in Appendix E.

Figure 5-1: Uphill Side Fatigue Crack Growth

Figure 5-2: Downhill Side Fatigue Crack Growth

Table 5-2: Contribution of Crack Growth from Individual Transients

	Uphill		Downhill	
Transient	Crack Growth	Percentage	Crack Growth	Percentage
	in		in	
1B	{	}	{	}
2B				
PL				
PU				
LeakTest				
LLA				
Insurge1				
Insurge2				
Insurge3				
Insurge4				
Insurge5				
Insurge6				
Insurge7				
Insurge8				
Insurge9				
Insurge10				
Insurge11				
Insurge12				
Insurge13				
Insurge14				
Total Crack Growth	{ } in	{ } Years	{ } in	40 Years

5.3 LEFM Evaluation

The LEFM evaluation was performed to determine LEFM safety margins. According to the LEFM criteria listed in Section 2.3, for normal and upset conditions, the applied safety margin should be greater than √10.

$$K_I < K_{Ia} / \sqrt{10}$$

The LEFM margins were calculated for all load steps. Table 5-3 lists only the time points that violated the LEFM criteria after { } years of plant operation for the uphill side. It is seen that for the uphill side transients 1A and 2A have the minimum LEFM safety margin of 1.2.

Table 5-4 lists the downhill LEFM evaluation, based on 40 year life. It is seen from Table 5-4 that the minimum LEFM margin of 2.6 occurs for transients 1A, 2A and Insurge1.

Table 5-3: Uphill LEFM Flaw Evaluation

Number of application years { } Crack depth { } in

Transient	Load Step	Temperature (F)	σ_y (ksi)	K initial KI (ksi√in)	K final, K_f ($KI\sqrt{a_f/a_0}$) (ksi√in)	Plasticity Correction $r_p=(1/6\pi)(K_f/\sigma_y)^2$ (in)	a_{eff} a_f+r_p (in)	KI_{eff} ($K_f\sqrt{a_{eff}/a_f}$) (ksi√in)	KI_a (ksi√in)	LEFM Margin KI_a/KI_{eff}
1A	1	70	50.0	16.7	34.6	0.0254		34.9	41.3	1.2
1B	1	70	50.0	14.5	30.2	0.0193		30.4	41.3	1.4
2A	17	70	50.0	16.7	34.6	0.0254		34.9	41.3	1.2
2B	27	70	50.0	14.6	30.2	0.0193		30.4	41.3	1.4
LeakTest	7	103	49.9	15.0	31.0	0.0205		31.2	50.2	1.6
Insrg1	5	628	41.7	55.7	115.5	0.4080		129.3	200.0	1.5
Insrg2	7	380	44.7	37.2	77.2	0.1585		80.9	200.0	2.5
Insrg3	9	633	41.6	51.0	105.7	0.3427		116.4	200.0	1.7
Insrg4	4	383	44.6	35.2	73.0	0.1419		76.1	200.0	2.6
Insrg5	5	382	44.6	34.2	71.0	0.1342		73.9	200.0	2.7
Insrg6	5	383	44.6	33.1	68.7	0.1257		71.3	200.0	2.8
Insrg7	7	636	41.6	45.4	94.1	0.2721		101.7	200.0	2.0
Insrg8	5	384	44.6	31.7	65.7	0.1150		68.0	200.0	2.9
Insrg9	5	383	44.6	30.6	63.4	0.1071		65.5	200.0	3.1
Insrg10	5	638	41.5	41.7	86.4	0.2297		92.4	200.0	2.2
Insrg11	7	637	41.6	39.7	82.4	0.2086		87.6	200.0	2.3

$KI_a = 26.8 + 12.445 \exp[0.0145 (T - RT_{NDT})]$

$KIc = 33.2 + 20.734 \exp[0.02 (T - RT_{NDT})]$

Table 5-4: Downhill LEFM Flaw Evaluation

Number of application years 40								Crack depth { } in		
Transient	Load Step	Temperature (F)	σ_y (ksi)	K initial KI (ksi√in)	K final, K_f ($KI\sqrt{a_f/a_0}$) (ksi√in)	Plasticity Correction $r_p=(1/6\pi)(K_f/\sigma_y)^2$ (in)	a_{eff} a_f+r_p (in)	KI_{eff} ($K_f\sqrt{a_{eff}/a_f}$) (ksi√in)	KI_a (ksi√in)	LEFM Margin KI_a/KI_{eff}
1A	1	70	50.0	10.2	15.8	0.0053		15.8	41.3	2.6
1B	1	70	50.0	7.1	11.0	0.0026		11.0	41.3	3.8
2A	17	70	50.0	10.2	15.8	0.0053		15.8	41.3	2.6
2B	27	70	50.0	7.1	11.0	0.0026		11.0	41.3	3.8
LeakTest	7	103	49.9	8.2	12.7	0.0034		12.7	50.3	3.9
Insurge1	5	605	41.9	46.6	72.2	0.1573		78.3	200.0	2.6
Insurge2	7	361	44.8	27.2	42.2	0.0471		43.3	200.0	4.6
Insurge3	9	614	41.8	42.6	65.9	0.1318		70.6	200.0	2.8
Insurge4	4	367	44.8	25.3	39.3	0.0408		40.1	200.0	5.0
Insurge5	5	365	44.8	24.6	38.2	0.0386		39.0	200.0	5.1
Insurge6	5	367	44.7	23.6	36.6	0.0355		37.3	200.0	5.4
Insurge7	7	620	41.8	38.0	58.8	0.1052		62.1	200.0	3.2
Insurge8	5	369	44.7	22.4	34.7	0.0320		35.3	200.0	5.7
Insurge9	5	368	44.7	21.6	33.4	0.0296		33.9	200.0	5.9
Insurge10	5	625	41.7	34.9	54.1	0.0892		56.7	200.0	3.5
Insurge11	7	623	41.7	33.5	51.8	0.0819		54.1	200.0	3.7

$KI_a = 26.8 + 12.445 \exp [0.0145 (T - RT_{NDT})]$

$KIc = 33.2 + 20.734 \exp [0.02 (T - RT_{NDT})]$

5.4 Screening Criteria for Flaw Evaluation

The screening criteria described in Section 2.4.1 was evaluated to determine the appropriated evaluation procedures for all the time points that was shown not to pass the LEFM criteria as shown in Table 5-3 and Table 5-4. Table 5-5 shows the results of evaluating the screening criteria for the uphill side. Based on the results shown in Table 5-5, the elastic-plastic fracture mechanics (EPFM) is the appropriated evaluation procedures for the flaw postulated in the uphill side.

Table 5-6 shows the results of evaluating the screening criteria for the downhill side. It is seen from the results summarized in Table 5-6 that a limit load analysis (LL) is appropriate for evaluating the flaw postulated in the downhill side. Since the limit load analysis is typically done for piping components which is different than the geometry of the component being analyzed, the elastic-plastic fracture mechanics (EPFM) flaw evaluation procedure will conservatively be used for evaluating the postulated downhill flaw.

Table 5-5: Uphill Screening Criteria

Number of application years { }							Crack depth { } in		
Transient	Load Step	σ_f (ksi)	KI_{eff} ($K_f\sqrt{a_{eff}/a_i}$) (ksi√in)	KI_C (ksi√in)	Kr' KI_{eff}/KI_C	σ_{max} (ksi)	sr' σ_{max}/σ_f	Kr'/Sr'	Appropriate Criteria
1A	1	65.0	34.9	58.5	0.596	51.1	0.787	0.76	EPFM
1B	1	65.0	30.4	58.5	0.519	49.1	0.755	0.69	EPFM
2A	17	65.0	34.9	58.5	0.596	51.1	0.787	0.76	EPFM
2B	27	65.0	30.4	58.6	0.519	49.1	0.755	0.69	EPFM
LeakTest	7	65.0	31.2	82.2	0.380	49.1	0.757	0.50	EPFM
Insurge1	5	60.8	129.3	200.0	0.646	129.4	2.128	0.30	EPFM
Insurge2	7	62.3	80.9	200.0	0.404	101.3	1.626	0.25	EPFM
Insurge3	9	60.8	116.4	200.0	0.582	118.3	1.946	0.30	EPFM
Insurge4	4	62.3	76.1	200.0	0.381	97.5	1.565	0.24	EPFM
Insurge5	5	62.3	73.9	200.0	0.369	94.9	1.523	0.24	EPFM
Insurge6	5	62.3	71.3	200.0	0.357	92.8	1.490	0.24	EPFM
Insurge7	7	60.8	101.7	200.0	0.509	105.1	1.729	0.29	EPFM
Insurge8	5	62.3	68.0	200.0	0.340	89.6	1.437	0.24	EPFM
Insurge9	5	62.3	65.5	200.0	0.327	86.9	1.395	0.23	EPFM
Insurge10	5	60.8	92.4	200.0	0.462	96.3	1.585	0.29	EPFM
Insurge11	7	60.8	87.6	200.0	0.438	91.6	1.507	0.29	EPFM

$KIc = 33.2 + 20.734 \exp [0.02 (T - RT_{NDT})]$

Table 5-6: Downhill Screening Criteria

Number of application years 40 | Crack depth {   } in

Transient	Load Step	σ_f (ksi)	KI_{eff} ($K_f\sqrt{a_{eff}/a_i}$) (ksi$\sqrt{in}$)	KI_C (ksi$\sqrt{in}$)	Kr' KI_{eff}/KI_C	σ_{max} (ksi)	sr' σ_{max}/σ_f	Kr'/Sr'	Appropriate Criteria
1A	1	65.0	15.8	58.5	0.270	47.7	0.735	0.37	EPFM
1B	1	65.0	11.0	58.5	0.188	46.4	0.714	0.26	EPFM
2A	17	65.0	15.8	58.5	0.270	47.7	0.735	0.37	EPFM
2B	27	65.0	11.0	58.6	0.188	46.4	0.715	0.26	EPFM
LeakTest	7	65.0	12.7	82.4	0.155	46.4	0.715	0.22	EPFM
Insurge1	5	61.0	78.3	200.0	0.391	224.3	3.679	0.11	LL
Insurge2	7	62.4	43.3	200.0	0.216	155.9	2.499	0.09	LL
Insurge3	9	60.9	70.6	200.0	0.353	200.9	3.298	0.11	LL
Insurge4	4	62.4	40.1	200.0	0.201	145.1	2.327	0.09	LL
Insurge5	5	62.4	39.0	200.0	0.195	139.0	2.228	0.09	LL
Insurge6	5	62.4	37.3	200.0	0.187	133.2	2.135	0.09	LL
Insurge7	7	60.9	62.1	200.0	0.311	173.1	2.843	0.11	LL
Insurge8	5	62.4	35.3	200.0	0.177	124.8	2.001	0.09	LL
Insurge9	5	62.4	33.9	200.0	0.170	118.3	1.897	0.09	LL
Insurge10	5	60.9	56.7	200.0	0.283	154.7	2.542	0.11	LL
Insurge11	7	60.9	54.1	200.0	0.271	144.6	2.377	0.11	LL

$KIc = 33.2 + 20.734 \exp[0.02 (T - RT_{NDT})]$

5.5 Uphill EPFM Flaw Evaluations

Based on the results provided in Section 5.4, the elastic-plastic fracture mechanics (EPFM) procedure described in Section 2.4 is used to evaluate the final size of the postulated flaw after fatigue crack growth. The EPFM results for the uphill flaw are shown in Table 5-7. The first part of Table 5-7 shows the applied J integral and Tearing modulus using a factor of safety of 3 on pressure stress and 1.5 on thermal and residual stress. The second part of Table 5-7 shows the J integral and Tearing modulus at the instability point. The instability point is found by iteratively changing the safety margin until the applied Tearing modulus and J integral are equal to the material Tearing modulus and J integral. Also, the second part of Table 5-7 shows the crack driving force evaluation where the applied J integral is evaluated using a factor of safety of 1.5 on pressure stress and 1.0 on thermal and residual stress. This value of applied J integral should remain below the material J integral at 0.1 in of stable crack extension. Based on the data reported in Table 5-7, the uphill flaw meets the EPFM evaluation criteria for { } years. The lowest margin (predicted by $J_{instability}/J_{applied}$) occurs for transient Insurge1 at load step 5. Detailed EPFM evaluation for this condition is shown in Table 5-8. Figure 5-3 shows the J-T diagram for this condition.

Table 5-7: Uphill EPFM Flaw Evaluation

Number of application years { }					Crack depth, a_f = { } in			
Transient	Load Step	Pressure,P (psi)	E' (ksi)	KI_p (ksi√in)	KIs KI_f-KI_p (ksi√in)	J_{app} (kip/in)	T_{app}	T_{mat}
1A	1	485	30659	6.9	27.7	0.128	0.525	1380.266
1B	1	85	30659	1.2	29.0	0.073	0.300	3728.151
2A	17	485	30659	6.9	27.7	0.128	0.525	1380.266
2B	27	85	30659	1.2	29.0	0.073	0.300	3726.325
LeakTest	7	345	30599	4.9	26.1	0.096	0.394	2296.337
Insurge1	5	2250	27961	32.1	83.4	2.198	9.360	9.384
Insurge2	7	247	29759	3.5	73.7	0.541	2.335	118.489
Insurge3	9	2250	27913	32.1	73.6	1.858	7.904	12.721
Insurge4	4	247	29744	3.5	69.5	0.482	2.080	145.853
Insurge5	5	247	29750	3.5	67.5	0.455	1.964	161.793
Insurge6	5	247	29746	3.5	65.2	0.425	1.835	182.700
Insurge7	7	2250	27884	32.1	62.0	1.503	6.394	18.665
Insurge8	5	247	29742	3.5	62.2	0.388	1.676	215.041
Insurge9	5	247	29747	3.5	59.9	0.361	1.560	244.708
Insurge10	5	2250	27863	32.1	54.3	1.297	5.515	24.384
Insurge11	7	2250	27877	32.1	50.3	1.196	5.085	28.270

C={ }

$KI_f = KI \times \sqrt{(a_f / a_0)}$ where a_f is the final flaw size and a_0 is the initial flaw size

$KI_p = (P/Pd) KI_{Po} \sqrt{(a_f / a_0)}$ where Pd = 2485 psi and KI_{po} is from Appendix D.

$a_e = a_f + (1 / 6\pi) * ((KI_p + KI_S) / \sigma_y)^2$

$KIp_{eff} = KI_p \times \sqrt{(a_e / a)}$

$KIs_{eff} = KI_S \times \sqrt{(a_e / a)}$

$J_{app} = (SFp \times KIp_{eff} + SF_s \times KIs_{eff})^2 / E'$ where SF_p=3 and SF_s = 1.5

$T_{app} = (E/\sigma_f^2)\,(J_{app}(a+.01) - J_{app}(a-.01))/.02$

$T_{mat} = (E/\sigma_f^2)\, Cm\, (\Delta a)^{m-1}$ where $\Delta a=(J/C)^{1/m}$

Table 5-7: Uphill EPFM Flaw Evaluation **(Continued)**

				Instability			Crack Driving Force	
Transient	Load Step	SFp=SFs	$J_{Instability}$	$T_{Instability}$ (kip/in)	m	T_{mat}	J_{app} (kip/in)	$J_{0.1}$ $C(0.1)^m$ (kip/in)
1A	1	7.461	2.206	9.019		9.019	0.048	1.167
1B	1	8.562	2.206	9.019		9.019	0.031	1.167
2A	17	7.461	2.206	9.019		9.019	0.048	1.167
2B	27	8.561	2.206	9.019		9.019	0.031	1.167
LeakTest	7	8.315	2.206	9.013		9.013	0.037	1.167
Insurge1	5	1.918	2.200	9.368		9.368	0.776	1.182
Insurge2	7	3.165	2.202	9.506		9.506	0.230	1.177
Insurge3	9	2.129	2.200	9.361		9.361	0.644	1.182
Insurge4	4	3.361	2.202	9.505		9.505	0.204	1.177
Insurge5	5	3.464	2.202	9.506		9.506	0.193	1.177
Insurge6	5	3.589	2.202	9.506		9.506	0.180	1.177
Insurge7	7	2.434	2.200	9.356		9.356	0.509	1.182
Insurge8	5	3.764	2.202	9.505		9.505	0.164	1.177
Insurge9	5	3.909	2.202	9.506		9.506	0.152	1.177
Insurge10	5	2.680	2.200	9.353		9.353	0.431	1.182
Insurge11	7	2.828	2.200	9.355		9.355	0.393	1.182

C={ }

$a_e = a_f + (1 / 6\pi) \times ((KI_p + KI_S) / \sigma_y)^2$

$KIp_{eff} = KI_p \times \sqrt{(a_e / a)}$

$KIs_{eff} = KI_S \times \sqrt{(a_e / a)}$

$J_{app} = (SFp \times KIp_{eff} + SF_s \times KIs_{eff})^2 / E'$ where $SF_p = 1.5$ and $SF_s = 1.0$

$T_{app} = (E/\sigma_f^2) (J_{app}(a+.01) - J_{app}(a-.01))/.02$

$T_{mat} = (E/\sigma_f^2)\ Cm\ (\Delta a)^{m-1}$ where $\Delta a=(J/C)^{1/m}$

Table 5-8: Detailed EPFM Evaluation for Transient Insurge1 Load Step 5 (Uphill)

EPFM Equations:

$J_{mat} = C(\Delta a)^m$

$T_{mat} = (E/\sigma_f^2)*Cm(\Delta a)^{m-1}$

C = { }
m =

$J_{app} = (SF_p*K'_{Ip}+SF_s*K'_{Is})^2/E'$

$T_{app} = (E/\sigma_f^2)*(dJ_{app}/da)$

Ductile Crack Growth Stability Criterion: $T_{app} < T_{mat}$

At instability: $T_{app} = T_{mat}$

Safety Factors		$SF*K'_{Ip}$	$SF*K'_{Is}$	J_{app}	T_{app}	Stable?
Primary	Secondary	(ksi√in)	(ksi√in)	(kips/in)		
1.00	1.00	35.972	93.325	0.598	2.546	Yes
2.00	1.00	71.945	93.325	0.977	4.160	Yes
3.00	1.50	107.917	139.988	2.198	9.360	Yes
5.00	1.00	179.862	93.325	2.669	11.367	NO
7.00	1.00	251.807	93.325	4.260	18.142	NO

Iterate on safety factor until $T_{app} = T_{mat}$ to determine $J_{instability}$:

				$J_{instability}$	T_{app}	T_{mat}
1.9182	1.9182	69.001	179.013	2.200	9.368	9.368

at J_{mat} = 2.198 kips/in, T_{mat} = 9.383

Applied J-Integral Criterion: $J_{app} < J_{0.1}$

where, $J_{0.1} = J_{mat}$ at Δa = 0.1 in.

Safety Factors		$SF*K'_{Ip}$	$SF*K'_{Is}$	J_{app}	$J_{0.1}$	OK?
Primary	Secondary	(ksi√in)	(ksi√in)	(kips/in)	(kips/in)	
1.50	1.00	53.959	93.325	0.776	1.182	Yes

Figure 5-3: J-T Diagram for Transient Insurge1 Load Step 5 (Uphill)

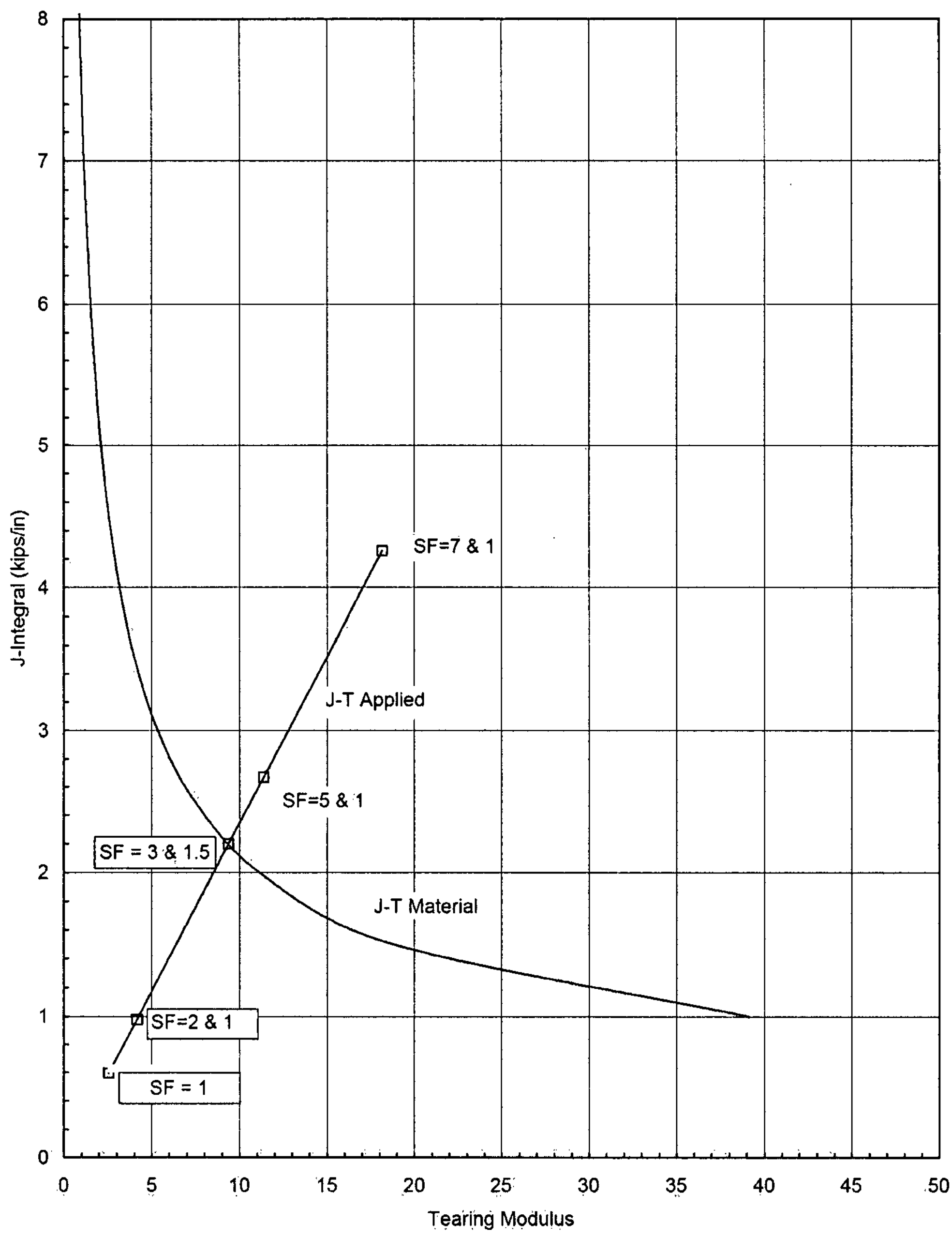

5.6 Downhill EPFM Flaw Evaluations

Based on the discussion provided in 5.4, elastic-plastic fracture mechanics (EPFM) procedure described in Section 2.4 is conservatively used to evaluate the final size of the postulated downhill flaw after fatigue crack growth. The EPFM results for the downhill flaw are shown in Table 5-9. The first part of Table 5-9 shows the applied J integral and Tearing modulus using a factor of safety of 3 on pressure stress and 1.5 on thermal and residual stress. The second part of Table 5-9 shows the J integral and Tearing modulus at the instability point. The instability point is found by iteratively changing the safety margin until the applied Tearing modulus and J integral are equal to the material Tearing modulus and J integral. Also, the second part of Table 5-9 shows the crack driving force evaluation where the applied J integral is evaluated using a factor of safety of 1.5 on pressure stress and 1.0 on thermal and residual stress. This value of applied J integral should remain below the material J integral at 0.1 in of stable crack extension. Based on the data reported in Table 5-9, the downhill flaw meets the EPFM evaluation criteria for 40 years. The lowest margin (predicted by Jinstability/Japplied) occurs for transient Insurge1 at load step 5. Detailed EPFM evaluation for this condition is shown in Table 5-10. Figure 5-4 shows the J-T diagram for this condition.

Table 5-9: Downhill EPFM Flaw Evaluation

Number of application years 40   Crack depth {   } in

Transient	Load Step	Pressure,P (psi)	E' (ksi)	KI_p (ksi√in)	KIs KI_f-KI_p (ksi√in)	J_{app} (kip/in)	T_{app}	T_{mat}
1A	1	485	30659	5.8	10.0	0.034	0.251	14308.913
1B	1	85	30659	1.0	10.0	0.011	0.078	113893.316
2A	17	485	30659	5.8	10.0	0.034	0.251	14308.913
2B	27	85	30659	1.0	10.0	0.011	0.078	113844.487
LeakTest	7	345	30599	4.1	8.6	0.021	0.153	34355.462
Insurge1	5	2250	28193	26.8	45.4	0.919	7.046	45.736
Insurge2	7	247	29842	2.9	39.3	0.162	1.253	1036.254
Insurge3	9	2250	28108	26.8	39.2	0.789	6.042	60.234
Insurge4	4	247	29817	2.9	36.3	0.141	1.089	1334.363
Insurge5	5	247	29824	2.9	35.2	0.133	1.031	1471.652
Insurge6	5	247	29815	2.9	33.7	0.123	0.952	1700.247
Insurge7	7	2250	28043	26.8	32.0	0.656	5.020	84.053
Insurge8	5	247	29808	2.9	31.8	0.111	0.859	2044.163
Insurge9	5	247	29813	2.9	30.5	0.103	0.797	2335.356
Insurge10	5	2250	27999	26.8	27.3	0.577	4.414	105.988
Insurge11	7	2250	28011	26.8	25.1	0.542	4.141	119.041

C={   }

$KI_f = KI \times \sqrt{(a_f / a_0)}$ where a_f is the final flaw size and a_0 is the initial flaw size

$K_{Ip} = (P/Pd) KI_{Po} \sqrt{(a_f / a_0)}$ where Pd = 2485 psi and KI_{po} is from Appendix D.

$a_e = a_f + (1 / 6\pi) * ((KI_p + KI_S) / \sigma_y)^2$

$KIp_{eff} = KI_p \times \sqrt{(a_e / a)}$

$KIs_{eff} = KI_S \times \sqrt{(a_e / a)}$

$J_{app} = (SFp \times KIp_{eff} + SF_s \times KIs_{eff})^2 / E'$ where $SF_p = 3.0$ and $SF_s = 1.5$

$T_{app} = (E/\sigma_f^2)\ (J_{app}(a+.01) - J_{app}(a-.01))/.02$

$T_{mat} = (E/\sigma_f^2)\ Cm\ (\Delta a)^{m-1}$ where $\Delta a = (J/C)^{1/m}$

Table 5-9: Downhill EPFM Flaw Evaluation (Continued)

			Instability				Crack Driving Force	
Transient	Load Step	SFp=SFs	$J_{Instability}$ (kip/in)	$T_{Instability}$	m	T_{mat}	J_{app} (kip/in)	$J_{0.1}$ $C(0.1)^m$ kip/in
1A	1	14.796	1.786	13.103		13.103	0.011	1.167
1B	1	21.257	1.786	13.103		13.103	0.004	1.167
2A	17	14.796	1.786	13.103		13.103	0.011	1.167
2B	27	21.254	1.786	13.103		13.103	0.004	1.167
LeakTest	7	18.343	1.786	13.096		13.096	0.007	1.167
Insurge1	5	2.867	1.787	13.704		13.704	0.305	1.182
Insurge2	7	5.333	1.787	13.847		13.847	0.067	1.176
Insurge3	9	3.174	1.787	13.686		13.686	0.257	1.182
Insurge4	4	5.749	1.787	13.845		13.845	0.058	1.176
Insurge5	5	5.919	1.787	13.845		13.845	0.055	1.176
Insurge6	5	6.181	1.787	13.844		13.844	0.051	1.176
Insurge7	7	3.603	1.787	13.672		13.672	0.208	1.182
Insurge8	5	6.532	1.787	13.844		13.844	0.045	1.176
Insurge9	5	6.800	1.787	13.844		13.844	0.042	1.176
Insurge10	5	3.946	1.787	13.663		13.663	0.179	1.182
Insurge11	7	4.133	1.787	13.666		13.666	0.166	1.182

C={ }

$a_e = a_f + (1 / 6\pi) \times ((KI_p + KI_S) / \sigma_y)^2$

$KIp_{eff} = KI_p \times \sqrt{(a_e / a)}$

$KIs_{eff} = KI_S \times \sqrt{(a_e / a)}$

$J_{app} = (SFp \times KIp_{eff} + SF_s \times KIs_{eff})^2 / E'$ where SF_p= 1.5 and SF_s = 1.0

$T_{app} = (E/\sigma_f^2)\ (J_{app}(a+.01) - J_{app}(a-.01))/.02$

$T_{mat} = (E/\sigma_f^2)\ Cm\ (\Delta a)^{m-1}$ where $\Delta a=(J/C)^{1/m}$

Table 5-10: Detailed EPFM Evaluation for Transient Insurge1 Load Step 5 (Downhill)

EPFM Equations:

$J_{mat} = C(\Delta a)^m$ C = { }

$T_{mat} = (E/\sigma_f^2)*Cm(\Delta a)^{m-1}$ m =

$J_{app} = (SF_p*K'_{Ip}+SF_s*K'_{Is})^2/E'$

$T_{app} = (E/\sigma_f^2)*(dJ_{app}/da)$

Ductile Crack Growth Stability Criterion: $T_{app} < T_{mat}$

At instability: $T_{app} = T_{mat}$

Safety Factors		$SF*K'_{Ip}$	$SF*K'_{Is}$	J_{app}	T_{app}	Stable?
Primary	Secondary	(ksi√in)	(ksi√in)	(kips/in)		
1.00	1.00	29.021	49.261	0.217	1.667	Yes
2.00	1.00	58.042	49.261	0.408	3.132	Yes
3.00	1.50	87.063	73.892	0.919	7.046	Yes
5.00	1.00	145.106	49.261	1.340	10.275	Yes
7.00	1.00	203.148	49.261	2.260	17.328	NO

Iterate on safety factor until $T_{app} = T_{mat}$ to determine $J_{instability}$:

				$J_{instability}$	T_{app}	T_{mat}
2.8674	2.8674	83.215	141.252	1.787	13.704	13.704

at J_{mat} = 0.919 kips/in, T_{mat} = 45.736

Applied J-Integral Criterion: $J_{app} < J_{0.1}$

where, $J_{0.1} = J_{mat}$ at Δa = 0.1 in.

Safety Factors		$SF*K'_{Ip}$	$SF*K'_{Is}$	J_{app}	$J_{0.1}$	OK?
Primary	Secondary	(ksi√in)	(ksi√in)	(kips/in)	(kips/in)	
1.50	1.00	43.532	49.261	0.305	1.182	Yes

Figure 5-4: J-T Diagram for Transient Insurge1 Load Step 5 (Downhill)

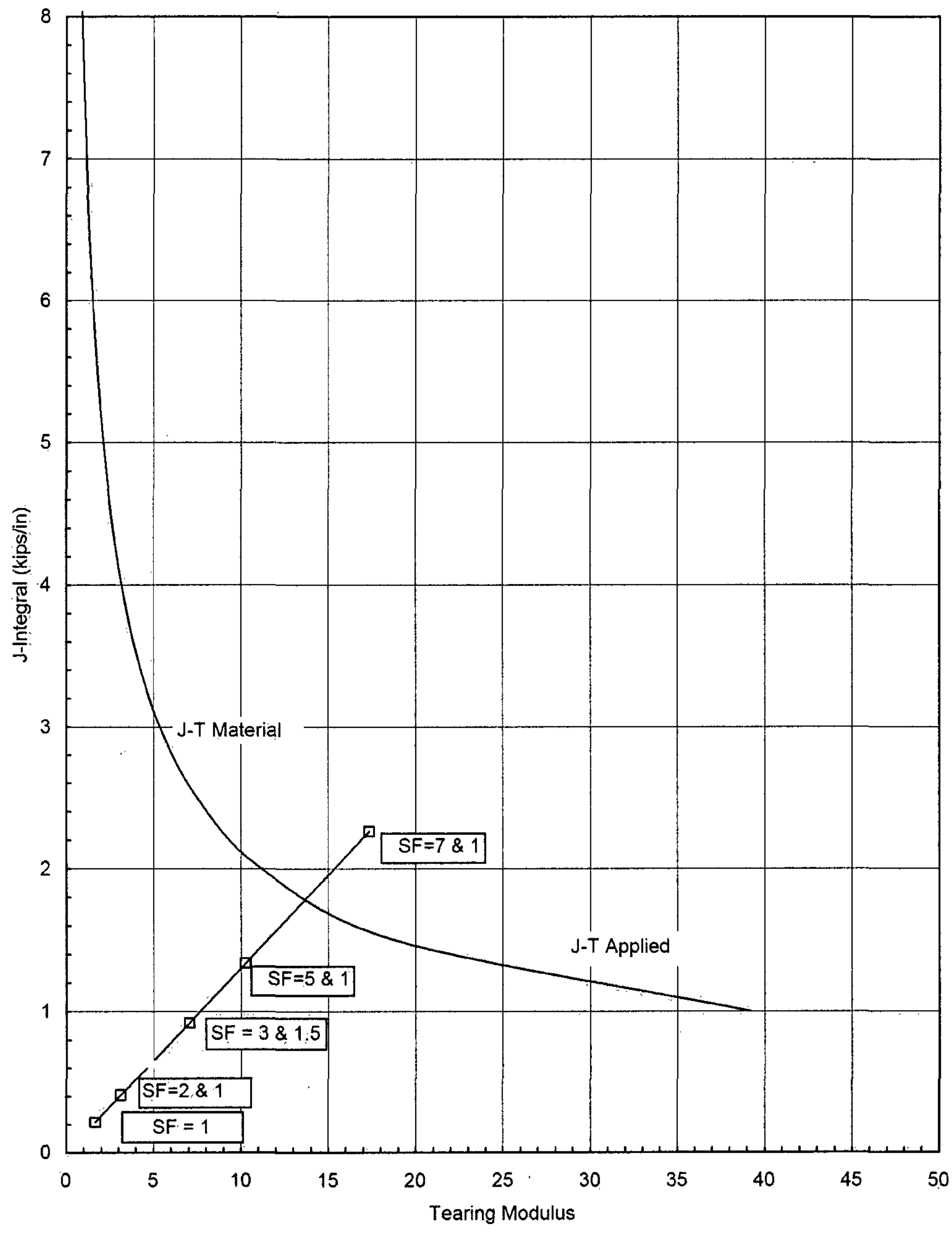

6.0 SUMMARY OF RESULTS AND CONCLUSIONS

Elastic-plastic fracture mechanics has been used to evaluate a postulated radial flaw in the J-groove weld and cladding of an outermost PZR heater sleeve penetration. The final flaw size was determined by linear-elastic fracture mechanics for { } years of fatigue crack growth.

6.1 Summary of Results

A summary of the results is provided in Table 6-1.

Table 6-1: Summary of Results

	Uphill Flaw	Downhill Flaw	
Initial flaw size	{ }	{ }	in
Time of fatigue crack growth	{ }	40	year
Final flaw size, af	{ }	{ }	in
Crack Growth	{ }	{ }	in
Safety factors (primary/secondary)	SF = 3 / 1.5		
Material tearing modulus	{ }	{ }	
Applied tearing modulus (< Tmat)	{ }	{ }	
Safety factors (primary/secondary)	SF = 1.5 / 1		
Material J-integral, $J_{0.1}$	{ }	{ }	kips/in
Applied J-integral (< $J_{0.1}$)	{ }	{ }	kips/in

6.2 Conclusion

Based on a combination of linear-elastic and elastic-plastic fracture mechanics analysis of a postulated remaining flaw in the original Alloy 82/182 J-groove weld and cladding, a remnant flaw in the CCNPP-1 heater sleeve penetration is considered to be acceptable for at least { } years of operation from the time the postulated flaw formed in the low alloy steel PZR lower head.

7.0 REFERENCES

1. AREVA NP Document, 08-9112221-002, Design Specification for Calvert Cliffs Unit 1, Pressurizer Heater Sleeve and Lower Instrumentation Nozzle Modification, September, 2009.
2. AREVA NP Drawing 02-9116243D-007, "Calvert Cliffs Pressurizer Heater Sleeve Nozzle Modification."
3. AREVA NP Document 51-5012047-00, "Stress Corrosion Cracking of Low Alloy Steel," March 2001.
4. ANSYS Finite Element Computer Code, Version 12.0, ANSYS Inc., Canonsburg, PA.
5. T.L. Anderson, Fracture Mechanics: Fundamentals and Applications, CRC Press, 1991.
6. AREVA Document 38-2200661-005, "Project Specification for a Pressurizer Assembly for Calvert Cliffs Units 1 & 2," VENDRPT# 20101112-00001.
7. ASME Boiler and Pressure Vessel Code, Section XI, Rules for Inservice Inspection of Nuclear Power Plant Components, 2004 Edition with no Addenda.
8. NUREG-0744, Vol. 2, Rev. 1, "Resolution of the Task A-11 Reactor Vessel Materials Toughness Safety Issue," Appendix D, Materials Toughness Properties, Division of Safety Technology, Office of Nuclear Reactor Regulation, U.S. Nuclear Regulatory Commission, Washington, D.C. 20555, October 1982.
9. AREVA NP Document 32-9126631-000, "Material and Transient Data for Pressurizer Heater Sleeve Repair Stress Analysis."
10. AREVA NP Document 32-9116466-003, "CCNPP-1 PZR Heater Sleeve & Plug Weld Residual Stress Analysis."
11. AREVA NP Document 32-9132487-005, "Calvert Cliffs Unit 1, Pressurizer Heater Sleeve/Plugged Sleeve Repair Structural Analysis."

APPENDIX A: VERIFICATION OF COMPUTER CODE ANSYS

The ANSYS finite element computer program [4] is verified for use in the present flaw evaluation by executing a test case from the ANSYS set of verification problems that utilize the SOLID186 structural 20-node 3-D solid elements. Test case VM256 determines stress intensity factors using ANSYS commands KCALC and CINT, for a crack in a plate using both 2D and 3D models. All test models executed properly, as demonstrated below for SOLID186 structural 3-D solid model. Also, a modified version of VM256 (VM256_Kcalc) was executed to verify that the UH_K1KCALC.mac and DH_K1KCALC files calculate the SIF similar to ANSYS KCALC routine. Results of verification test are listed below:

Verification Problem VM256
Fracture Mechanics Stress Intensity Calculation for a Semi Circular Surface Crack in a 3D Plate
File: vm256.vrt

```
-------------------- VM256 RESULTS COMPARISON --------------
               |  TARGET   |   ANSYS   |  RATIO
        ***************************************
         USING PLANE 183 ELEMENT (2-D ANALYSIS)
        ***************************************
           KI  1.0249      1.0038   0.979
               PRINTOUT RESUMED BY /GOP
        ***************************************
         USING SOLID 185 ELEMENT (3-D ANALYSIS)
        ***************************************
           KI  1.0249      1.0383   1.013
               PRINTOUT RESUMED BY /GOP
 ********************************************************
 USING SOLID 186 ELEMENT - SURFACE CRACK (3-D ANALYSIS)
 ********************************************************
           KI  1.4000      1.4132   1.009
------------------------------------------------------------
```

Verification Problem VM256_Kcalc

```
------------------- VM256_Kcalc RESULTS COMPARISON --------------
                  |  TARGET   |   ANSYS   |  RATIO
                |  Ansys Kcalc |   K1Kcalc_ver.mac
                PRINTOUT RESUMED BY /GOP
    ********************************************************
     USING SOLID 186 ELEMENT - SURFACE CRACK (3-D ANALYSIS)
    ********************************************************
        K1              314.7        312.9     0.99
    -------------------------------------------------------
```

APPENDIX B: COMPUTER USAGE

B.1 Software/Hardware

ANSYS Version 12.0 is used in this calculation. The hardware platform is Dell Precision PWS690, Intel® Xeon® CPU, 5160 @ 3.33GHz, 2.99GHz, 32.0 GB of RAM, Serial No. 9BHGZC1, and the Operating System is Microsoft Windows XP Professional x64 Edition Version 2003 Service Pack 1.

B.2 Computer Files

All ANSYS input/output files are collected as listed as follows. ANSYS verification input/output files are also listed. The computer files listed below have been placed in the AREVA NP COLDStor repository in the directory "\cold\41304\32-9116467-002\official". All files were installed on 1/20/2010.

For ANSYS 12.0, test case vm256 is run to verify that the answers are correct. The files vm256.vrt contains output from the test case. Review of the output shows that the test case is run successfully. ANSYS 12.0 analysis and verification files were run on Dell Precision PWS690, Tag# 9BHGZC1.

1. Computer program tested: ANSYS 12.0
2. Computer hardware used: Intel® Xeon® CPU, 5160 @ 3.33GHz, 2.99GHz Tag# 9BHGZC1
3. Name of person running test: Samer Mahmoud
4. Date of test: 06-15-2010
5. Results and acceptability: The results of test case vm256.vrt as listed in Appendix A are acceptable.

ANSYS Models

File Name	Description	Modified Date	Checksum
CCPZRHS_FM_Uhill.db	Crack model for uphill side	06/07/2010	30821
CCPZRHS_FM_Dhill.db	Crack model for downhill side	06/04/2010	19091

Files for Downhill Side Crack

File Name	Description	Modified Date	Checksum
DH_K1.out	Output file contains SIF (Downhill)	06/11/2010	15952
DH_K1_DC.out	Output file contains SIF (Downhill Design Case)	06/11/2010	31810
DH_K1Kcalc.mac	ANSYS command sets to calculate SIF	06/10/2010	12601
RUN_DH.inp	ANSYS command sets to run analysis results (Downhill)	06/10/2010	1333
RUN_DH.out	ANSYS output file (Downhill)	06/11/2010	35329
RUN_DH_DC.inp	ANSYS command sets to run analysis results (Downhill Design Case)	06/10/2010	10766
RUN_DH_DC.out	ANSYS output file (Downhill Design Case)	06/11/2010	26263
SummerizeResults.mac	ANSYS command sets to summarize results (Downhill)	06/04/2010	37552
SummerizeResults_DC.mac	ANSYS command sets to summarize results (Downhill Design Case)	06/08/2010	38405
sfmap_Prep.mac	ANSYS command sets to map stress	06/07/2010	18442

Files for Uphill Side Crack

File Name	Description	Modified Date	Checksum
UH_K1.out	Output file contains SIF (Uphill)	06/10/2010	51213
DC_UH_K1.out	Output file contains SIF (Uphill Design Case)	06/10/2010	21425
UH_K1Kcalc.mac	ANSYS command sets to calculate SIF	06/10/2010	8841
RUN_UH.inp	ANSYS command sets to run analysis (Uphill)	06/10/2010	52746
RUN_UH.out	ANSYS output file (Uphill)	06/10/2010	56757
RUN_UH_DC.inp	ANSYS command sets to run analysis results (Uphill Design Case)	06/10/2010	10603
RUN_UH_DC.out	ANSYS output file (Uphill Design Case)	06/10/2010	50226
UH_SummerizeResults.mac	ANSYS command sets to summarize results (Uphill)	06/07/2010	811
DC_UH_SummerizeResults.mac	ANSYS command sets to summarize results (Uphill Design Case)	06/09/2010	31076
sfmap_Prep.mac	ANSYS command sets to map stress	06/07/2010	18442

ANSYS Verification

File Name	Description	Modified Date	Checksum
VM256.inp	Input for verification problem for SIF calculation with SOLID 86	06-15-10	11797
vm256.vrt	Results for verification problem for SIF calculation with SOLID 86	06-15-10	49343
Vm256.out	Output for verification problem for SIF calculation with SOLID 86	06-15-10	29168
VM256_Kcalc.inp	Input for modified verification problem for K1Kcalc.mac ANSYS command sets	06-15-10	11000
VM256_Kcalc.vrt	Output for modified verification problem for K1Kcalc.mac ANSYS command sets	06-15-10	42538
VM256_Kcalc.out	Results for modified verification problem for K1Kcalc.mac ANSYS command sets	06-15-10	3483
K1Kcalc_ver.mac	ANSYS command sets to calculate SIF for verification case	06-15-10	61227

Excel Sheet Calculations

File Name	Description	Modified Date	Checksum
UH_K1.xls	Crack growth, LEFM , and EPFM evaluations for uphill side	09/17/2010	36837
DH_K1.xls	Crack growth, LEFM , and EPFM evaluations for downhill side	09/17/2010	63707

APPENDIX C: FINITE ELEMENT CRACK MODEL

C.1 Introduction

A non-radial partial penetration nozzle in a spherically shaped pressure vessel presents a challenging set of geometric constraints for both stress analysis and fracture mechanics analysis of flaws, especially in the J-groove weld. Since there are no closed-form solutions available to calculate stress intensity factors for such flaws, a three-dimensional finite element crack model is developed in this appendix for use in evaluating the postulated flaws in the area of the partial penetration attachment weld.

The three-dimensional finite element model is constructed using crack tip elements along the entire postulated crack fronts, extending from the inside surface of the cladding to the interface between the cladding and the low alloy steel lower head. An uncracked model of the, remnant heater sleeve, a portion of the PZR lower head and cladding is first created using the ANSYS finite element computer program [4]. After removing a block of elements around the crack front and inserting a sub-model of crack tip elements, stress intensity factors can be obtained via the program's KCALC routine or similar procedures. The crack tip sub-model consists of 20-node isoparametric elements that are collapsed to form wedges, with the appropriate mid-side nodes shifted to quarter-point locations to create a $1/\sqrt{r}$ singularity in strain at the crack tip.

C.2 Base Finite Element Model

A three-dimensional finite element model is constructed to represent an uncracked non-radial nozzle penetration in a hemi-spherical shaped head. This model utilizes the ANSYS SOLID186 3-D 20-node structural solid element, so that a portion of the model can be readily removed and replaced with a crack tip sub-model.

C.2.1 Geometry

As shown in Figure C-1, the model is a 180-degree segment of the head, cladding, and remnant heater sleeve.

Figure C-1: Overall Model of PZR Lower Head Penetration

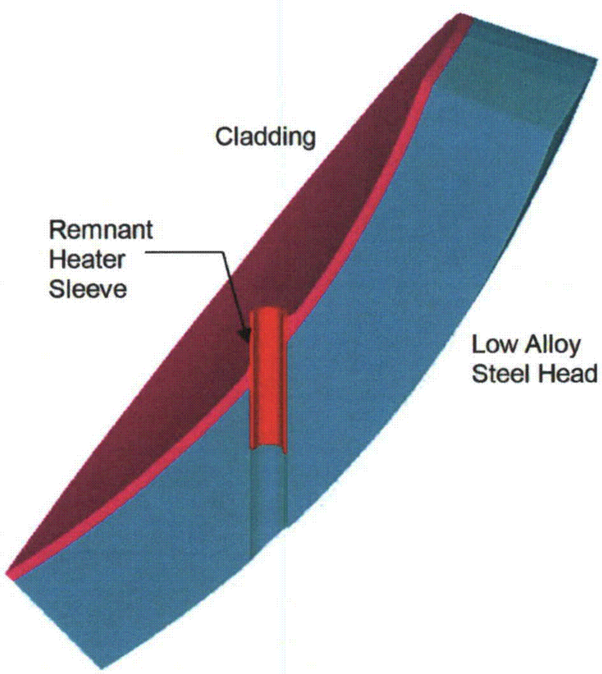

Key dimensions are:

Radius to base metal	= { } in.	[2]
Head thickness (minimum)	= { } in.	[2]
Cladding thickness (nominal)	= { } in.	[2]
Penetration bore	= { } in.	[2]
Penetration to PZR center	= { } in.	[2]
Initial flaw depth	= { } in	(equals to cladding thickness)

C.2.2 Materials

Component	Material
PZR bottom head	SA-533 Grade B Class 1 [1]
Cladding	Ni-Cr-Fe (use Alloy 600) [1]
J-groove weld filler	Alloy 82/182 (use Alloy 600) [1]
Existing Lower Level Heater Sleeve	SB-166, Alloy 600 [1]

The mechanical properties for these materials are provided in Section 4.1.1.

C.2.3 Boundary Conditions

The model includes a 180-degree segment of the PZR heater sleeve and portions of the head. The vertical plane containing the vertical axes of the PZR and the outermost heater sleeve penetration forms a plane of symmetry for the model. The displacements normal to this plane of symmetry are fixed (in the global Z-direction). Displacement constraints are also applied to the outer peripheral boundary of the spherical segment to simulate a state of membrane stress. By specifying meridional displacements to be zero in a spherical coordinate system, the head can only displace along a spherical radius parallel to this boundary.

C.3 Finite Element Crack Models

The three-dimensional finite element crack model is developed by removing a portion of the head cladding and inserting a sub-model of crack tip elements, as illustrated in Figure C-2. Displacement constraints are also removed along the plane of symmetry for nodes on the crack face. Figure C-3 shows the final crack models for both downhill and uphill sides used to analyze a postulated flaw in the PZR lower head.

Figure C-2: Development of Crack Model

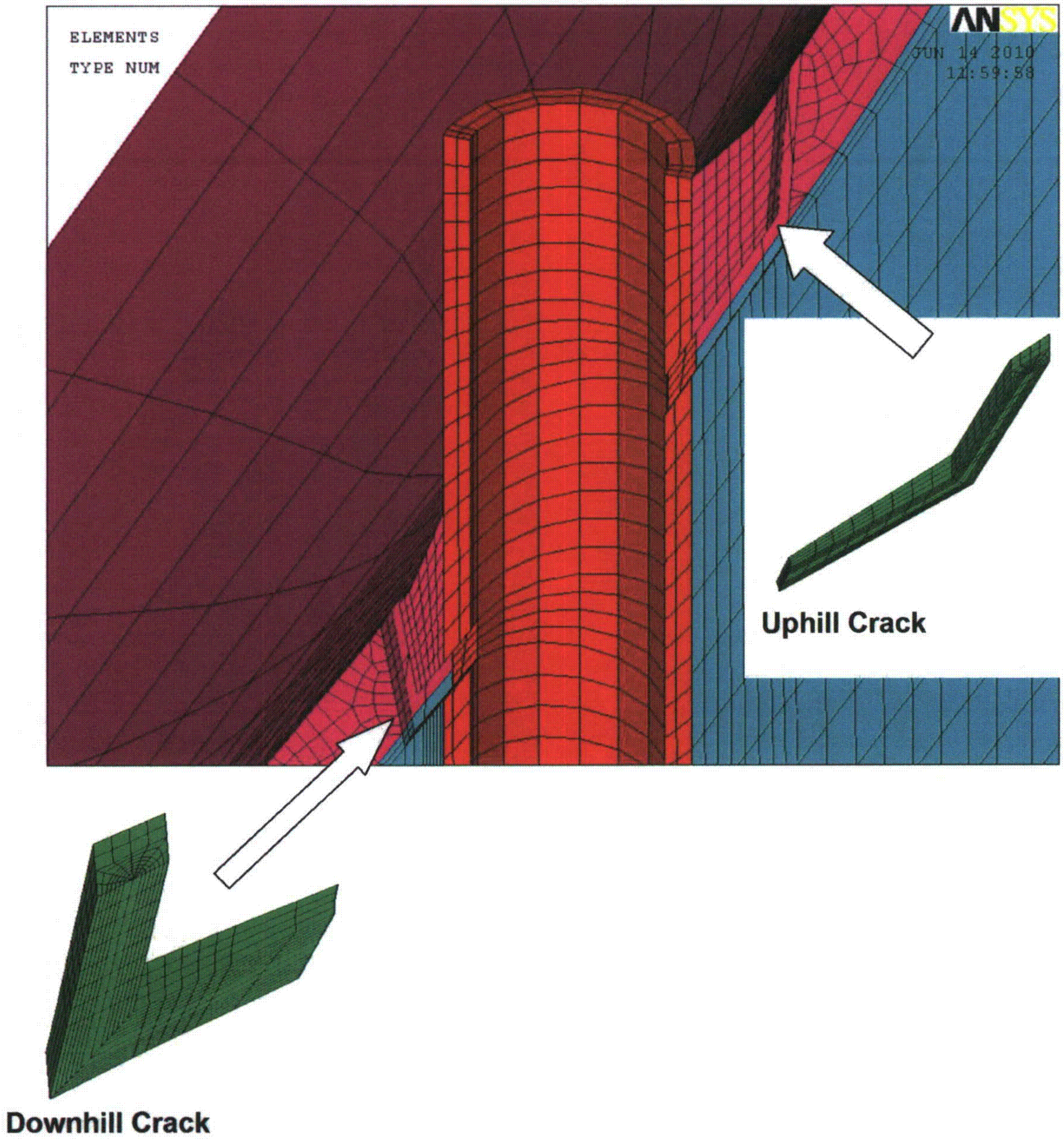

Figure C-3: Final Finite Element Crack Models

Downhill Crack

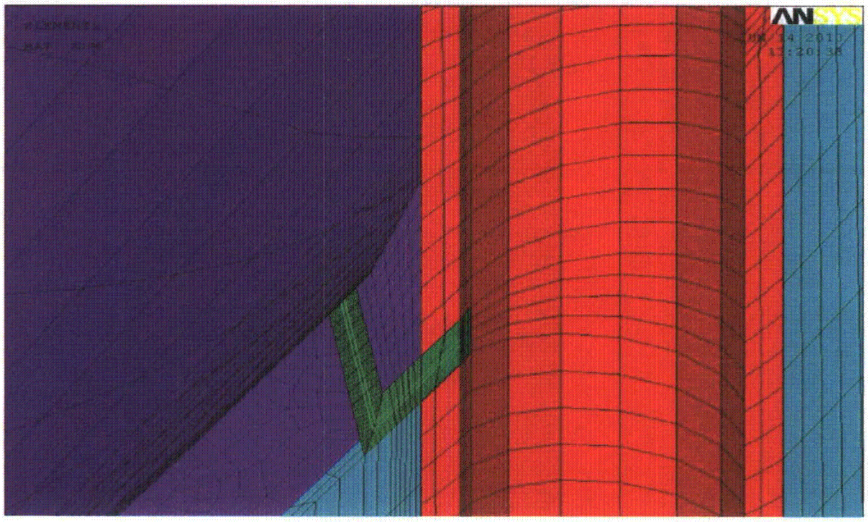

Uphill Crack

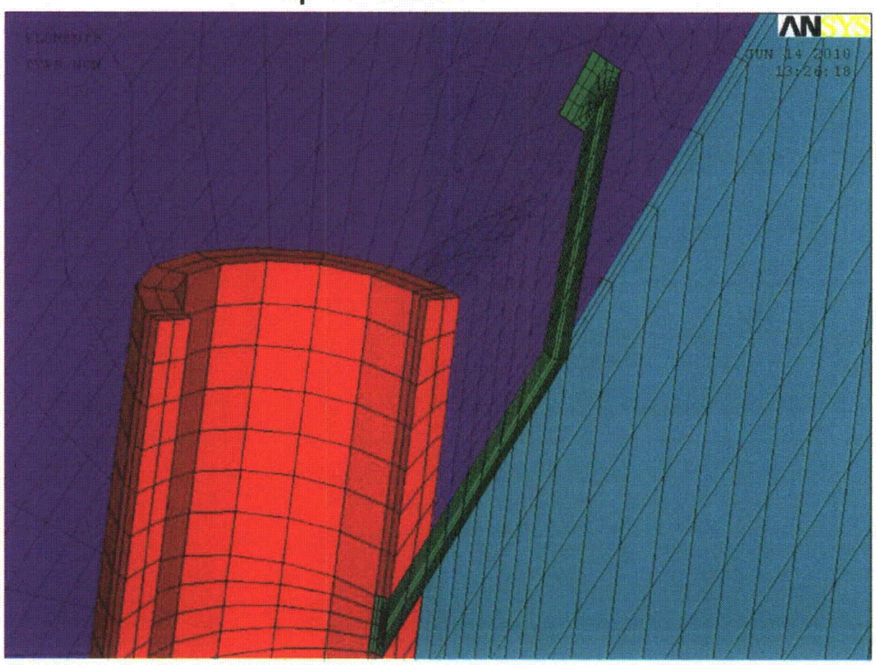

APPENDIX D: STRESS INTENSITY FACTOR DUE TO PRESSURE

The elastic-plastic fracture flaw evaluations of Section 2.4 utilize different safety factors for primary (pressure) and secondary stress (residual and thermal) intensity factors. In order to isolate the pressure term, K_{Ip}, stress intensity factors are developed for the design case conditions (pressure load of { } psig at { } °F) where the uncracked stress values are obtained from Reference [11]. Table D-1 and Table D-2 presents stress intensity factors at all crack front positions defined in Figure 2-3 and Figure 2-4 for both downhill and uphill postulated cracks. Since these values were determined for the initial crack size, they are adjusted by the square root of the crack size, considering the final crack size after crack growth, in the same fashion as described in Section 2.2.

The K_{Ip} pressure terms used in the EPFM flaw evaluations of Section 5.5 are derived below.

Let,

$$K_{Ip}(a,P) = K_{Ip}(a_o,P_o)\sqrt{\frac{a}{a_o}} \times \frac{P}{P_o}$$

Temperature, $T = \{ \quad \}\ ^\circ F$

Pressure, $P_o = \{ \quad \}$ psig

Initial flaw size, $a_o = \{ \quad \}$ in.

From Table D-1, the downhill pressure stress intensity factor is evaluated at crack tip 15 to be { } psi √in which is the highest pressure stress intensity factor in the low alloy head.

From Table D-2, the uphill pressure stress intensity factor is evaluated at crack tip 13 to be { } psi √in which is the highest pressure stress intensity factor in the low alloy head.

Table D-1: Downhill Stress Intensity Factors for Design Case Pressure

	Position	SIF (psi√ in)
Insied Surface	1	45878.1
	2	28322.6
	3	24322.0
	4	21765.6
	5	20045.1
	6	18195.0
	7	16118.9
	8	13640.3
	9	3078.3
	10	10325.1
	11	11683.3
	12	13008.3
	13	15182.7
	14	17664.2
Bore Surface	15	19088.3
	16	18270.1
Nozzle ID	17	37552.8

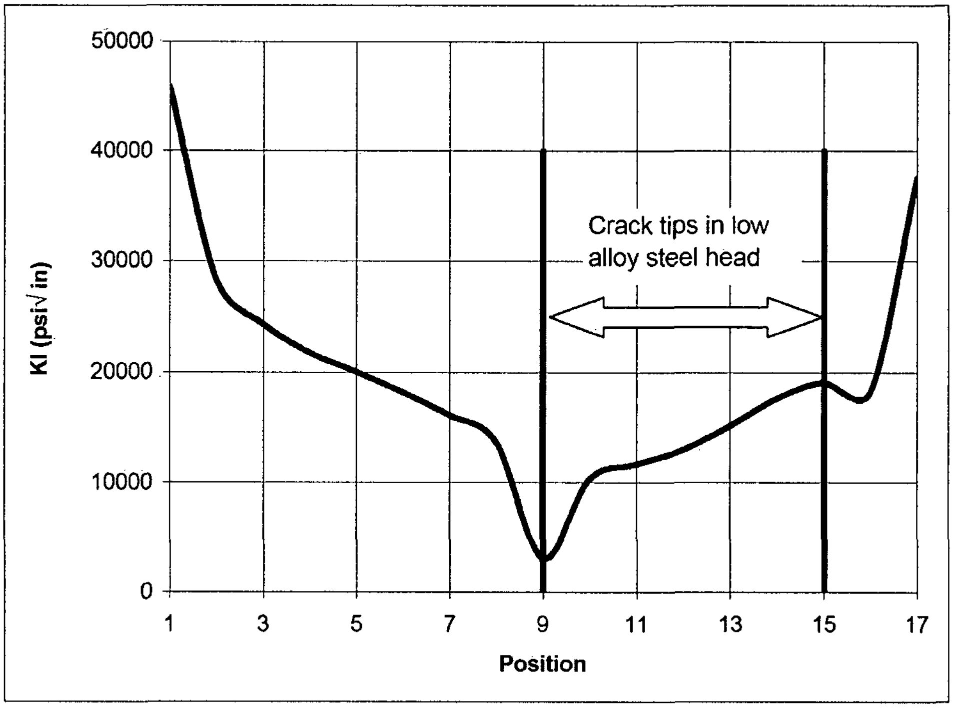

Table D-2: Uphill Stress Intensity Factors for Design Case Pressure

Temperature = { } F
Pressure = psig
Flaw size = in

	Position	SIF (psi√ in)
Insied Surface	1	2880.1
	2	6621.0
	3	8519.0
	4	9964.7
	5	11101.0
	6	12013.4
	7	12626.8
	8	12974.0
	9	12980.9
	10	15803.6
	11	14823.3
	12	16054.8
	13	17106.3
	14	16944.6
	15	15037.5
Bore Surface	16	15619.9
	17	9552.1
Nozzle ID	18	6518.6

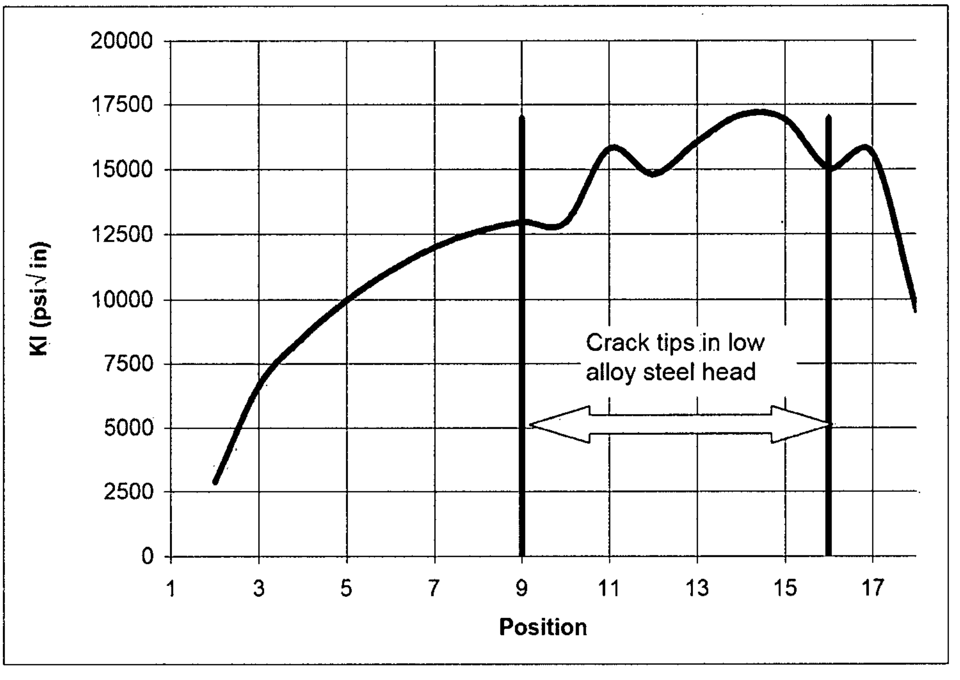

APPENDIX E: DETAILED CRACK GROWTH CALCULATIONS

Table E-1: Uphill Detailed Crack Growth

FATIGUE CRACK GROWTH

a0
a0= in
af= in
500.000 cycles 40 years
ΔN 12.500 cycles/year
Transient 1B

Year of Operation	a (in.)	Position 13 Kmin KI(a) (ksi√in)	Kmax KI(a) (ksi√in)	Δa (in.)
		3.1		
		3.1		
		3.2		
		3.3		
		3.3		
		3.4		
		3.5		
		3.5		
		3.6		
		3.7		
		3.8		
		3.8		
		3.9		
		4.0		
		4.1		
		4.2		
		4.3		
		4.4		
		4.5		
		4.6		
		4.6		
		4.7		
		4.8		
		4.9		
		5.1		
		5.2		
		5.3		
		5.4		
		5.5		
		5.6		
		5.7		
		5.8		
		6.0		
		6.1		
		6.2		

FATIGUE CRACK GROWTH

a0= in
af= in
500.000 cycles 40 years
ΔN 12.500 cycles/year
Transient 2B

Year of Operation	a (in.)	Position 13 Kmin KI(a) (ksi√in)	Kmax KI(a) (ksi√in)	Δa (in.)
		8.3	18.2	
		8.4	18.6	
		8.6	19.0	
		8.8	19.4	
		9.0	19.8	
		9.2	20.2	
		9.4	20.6	
		9.5	21.1	
		9.8	21.5	
		10.0	22.0	
		10.2	22.4	
		10.4	22.9	
		10.6	23.4	
		10.8	23.9	
		11.1	24.4	
		11.3	24.9	
		11.5	25.4	
		11.8	26.0	
		12.0	26.5	
		12.3	27.1	
		12.5	27.7	
		12.8	28.2	
		13.1	28.8	
		13.4	29.4	
		13.6	30.1	
		13.9	30.7	
		14.2	31.3	
		14.5	32.0	
		14.8	32.7	
		15.1	33.4	
		15.5	34.1	
		15.8	34.8	
		16.1	35.5	
		16.4	36.3	
		16.8	37.0	

FATIGUE CRACK GROWTH

a0= in
af= in
15000.000 cycles 40 years
ΔN 375.000 cycles/year
Transient PL

Year of Operation	a (in.)	Position 10 Kmin KI(a) (ksi√in)	Kmax KI(a) (ksi√in)	Δa (in.)
		21.7	23.7	
		22.2	24.2	
		22.7	24.7	
		23.1	25.2	
		23.6	25.7	
		24.1	26.3	
		24.6	26.8	
		25.1	27.4	
		25.7	28.0	
		26.2	28.6	
		26.8	29.2	
		27.3	29.8	
		27.9	30.4	
		28.5	31.1	
		29.1	31.7	
		29.8	32.4	
		30.4	33.1	
		31.0	33.8	
		31.7	34.5	
		32.4	35.3	
		33.0	36.0	
		33.7	36.8	
		34.4	37.5	
		35.2	38.3	
		35.9	39.1	
		36.7	40.0	
		37.4	40.8	
		38.2	41.7	
		39.0	42.5	
		39.9	43.4	
		40.7	44.3	
		41.5	45.3	
		42.4	46.2	
		43.3	47.2	
		44.2	48.2	

FATIGUE CRACK GROWTH

a0= { } in
af= { } in
15000.000 cycles 40 years
ΔN 375.000 cycles/year
Transient PU

Year of Operation	a (in.)	Position 10 Kmin KI(a) (ksi√in)	Kmax KI(a) (ksi√in)	Δa (in.)
		21.8	24.0	
		22.3	24.5	
		22.7	25.0	
		23.2	25.5	
		23.7	26.0	
		24.2	26.6	
		24.7	27.1	
		25.2	27.7	
		25.8	28.3	
		26.3	28.9	
		26.9	29.5	
		27.4	30.2	
		28.0	30.8	
		28.6	31.4	
		29.2	32.1	
		29.8	32.8	
		30.5	33.5	
		31.1	34.2	
		31.8	34.9	
		32.4	35.7	
		33.1	36.4	
		33.8	37.2	
		34.6	38.0	
		35.3	38.8	
		36.0	39.6	
		36.8	40.4	
		37.6	41.3	
		38.3	42.2	
		39.1	43.0	
		40.0	43.9	
		40.8	44.9	
		41.7	45.8	
		42.5	46.8	
		43.4	47.7	
		44.3	48.7	

FATIGUE CRACK GROWTH

a0= { } in
af= { } in
320.000 cycles 40 years
ΔN 8.000 cycles/year
Transient LeakTest

Year of Operation	a (in.)	Position 13 Kmin KI(a) (ksi√in)	Kmax KI(a) (ksi√in)	Δa (in.)
		7.0	19.2	
		7.2	19.6	
		7.3	20.0	
		7.5	20.4	
		7.6	20.9	
		7.8	21.3	
		8.0	21.7	
		8.1	22.2	
		8.3	22.7	
		8.5	23.2	
		8.7	23.7	
		8.9	24.2	
		9.0	24.7	
		9.2	25.2	
		9.4	25.7	
		9.6	26.3	
		9.8	26.8	
		10.0	27.4	
		10.3	28.0	
		10.5	28.6	
		10.7	29.2	
		10.9	29.8	
		11.1	30.4	
		11.4	31.1	
		11.6	31.7	
		11.9	32.4	
		12.1	33.1	
		12.4	33.8	
		12.6	34.5	
		12.9	35.2	
		13.2	35.9	
		13.4	36.7	
		13.7	37.5	
		14.0	38.2	
		14.3	39.0	

FATIGUE CRACK GROWTH

a0= { } in
af= { } in
480.000 cycles 40 years
ΔN 12.000 cycles/year
Transient LLA

Year of Operation	a (in.)	Position 10 Kmin KI(a) (ksi√in)	Kmax KI(a) (ksi√in)	Δa (in.)
		18.7	24.6	
		19.1	25.1	
		19.5	25.6	
		19.9	26.2	
		20.3	26.7	
		20.7	27.3	
		21.2	27.9	
		21.6	28.4	
		22.1	29.0	
		22.6	29.7	
		23.0	30.3	
		23.5	30.9	
		24.0	31.6	
		24.5	32.3	
		25.1	33.0	
		25.6	33.7	
		26.1	34.4	
		26.7	35.1	
		27.2	35.8	
		27.8	36.6	
		28.4	37.4	
		29.0	38.2	
		29.6	39.0	
		30.3	39.8	
		30.9	40.6	
		31.5	41.5	
		32.2	42.4	
		32.9	43.3	
		33.6	44.2	
		34.3	45.1	
		35.0	46.0	
		35.7	47.0	
		36.5	48.0	
		37.2	49.0	
		38.0	50.0	

FATIGUE CRACK GROWTH

a0= { } in
af= { } in
60.000 cycles 40 years
ΔN 1.500 cycles/year
Transient Insurge1

Year of Operation	a (in.)	Position 10 Kmin KI(a) (ksi√in)	Kmax KI(a) (ksi√in)	Δa (in.)
		22.1	62.8	
		22.6	64.1	
		23.1	65.4	
		23.5	66.8	
		24.0	68.2	
		24.5	69.7	
		25.1	71.1	
		25.6	72.6	
		26.1	74.2	
		26.7	75.7	
		27.3	77.4	
		27.8	79.0	
		28.4	80.7	
		29.0	82.4	
		29.7	84.2	
		30.3	85.9	
		30.9	87.8	
		31.6	89.6	
		32.3	91.5	
		32.9	93.5	
		33.6	95.4	
		34.3	97.5	
		35.1	99.5	
		35.8	101.6	
		36.6	103.7	
		37.3	105.9	
		38.1	108.2	
		38.9	110.4	
		39.7	112.8	
		40.6	115.1	
		41.4	117.5	
		42.3	120.0	
		43.2	122.5	
		44.1	125.1	
		45.0	127.7	

FATIGUE CRACK GROWTH

a0= { } in
af= { } in
70.000 cycles 40 years
ΔN 1.750 cycles/year
Transient Insurge2

Year of Operation	a (in.)	Position 10 Kmin KI(a) (ksi√in)	Kmax KI(a) (ksi√in)	Δa (in.)
		11.0	43.9	
		11.2	44.8	
		11.4	45.8	
		11.7	46.7	
		11.9	47.7	
		12.2	48.7	
		12.4	49.7	
		12.7	50.8	
		12.9	51.9	
		13.2	53.0	
		13.5	54.1	
		13.8	55.2	
		14.1	56.4	
		14.4	57.6	
		14.7	58.8	
		15.0	60.1	
		15.3	61.4	
		15.6	62.7	
		16.0	64.0	
		16.3	65.4	
		16.7	66.7	
		17.0	68.1	
		17.4	69.6	
		17.7	71.1	
		18.1	72.5	
		18.5	74.1	
		18.9	75.6	
		19.3	77.2	
		19.7	78.8	
		20.1	80.5	
		20.5	82.2	
		21.0	83.9	
		21.4	85.7	
		21.8	87.5	
		22.3	89.3	

FATIGUE CRACK GROWTH

a0= { } in
af= { } in
130.000 cycles 40 years
ΔN 3.250 cycles/year
Transient Insurge3

Year of Operation	a (in.)	Position 10 Kmin KI(a) (ksi√in)	Kmax KI(a) (ksi√in)	Δa (in.)
		22.1	57.7	
		22.6	58.9	
		23.1	60.1	
		23.6	61.4	
		24.1	62.7	
		24.6	64.0	
		25.1	65.3	
		25.6	66.7	
		26.2	68.1	
		26.7	69.6	
		27.3	71.0	
		27.9	72.6	
		28.4	74.1	
		29.1	75.7	
		29.7	77.3	
		30.3	78.9	
		30.9	80.6	
		31.6	82.3	
		32.3	84.1	
		33.0	85.8	
		33.7	87.7	
		34.4	89.5	
		35.1	91.4	
		35.8	93.3	
		36.6	95.3	
		37.4	97.3	
		38.1	99.3	
		38.9	101.4	
		39.8	103.6	
		40.6	105.7	
		41.4	108.0	
		42.3	110.2	
		43.2	112.5	
		44.1	114.9	
		45.0	117.3	

CCNPP-1 PZR Heater Sleeve As-Left J-Groove Weld Flaw Evaluation for IDTB Repair

FATIGUE CRACK GROWTH

a0= { } in
af= { } in

	530.000	cycles	40	years
ΔN	13.250	cycles/year		
Transient	Insurge4			

Year of Operation	a (in.)	Position 10 Kmin KI(a) (ksi√in)	Kmax KI(a) (ksi√in)	Δa (in.)
		11.0	41.7	
		11.2	42.5	
		11.4	43.4	
		11.7	44.3	
		11.9	45.3	
		12.2	46.2	
		12.4	47.2	
		12.7	48.2	
		13.0	49.2	
		13.2	50.3	
		13.5	51.3	
		13.8	52.4	
		14.1	53.5	
		14.4	54.7	
		14.7	55.8	
		15.0	57.0	
		15.3	58.2	
		15.7	59.5	
		16.0	60.7	
		16.3	62.0	
		16.7	63.3	
		17.0	64.7	
		17.4	66.0	
		17.8	67.4	
		18.1	68.8	
		18.5	70.3	
		18.9	71.8	
		19.3	73.3	
		19.7	74.8	
		20.1	76.4	
		20.5	78.0	
		21.0	79.6	
		21.4	81.3	
		21.9	83.0	
		22.3	84.7	

FATIGUE CRACK GROWTH

a0= { } in
af= { } in

	120.000	cycles	40	years
ΔN	3.000	cycles/year		
Transient	Insurge5			

Year of Operation	a (in.)	Position 10 Kmin KI(a) (ksi√in)	Kmax KI(a) (ksi√in)	Δa (in.)
		11.0	40.6	
		11.2	41.5	
		11.4	42.3	
		11.7	43.2	
		11.9	44.1	
		12.2	45.0	
		12.4	46.0	
		12.7	47.0	
		13.0	48.0	
		13.2	49.0	
		13.5	50.0	
		13.8	51.1	
		14.1	52.2	
		14.4	53.3	
		14.7	54.4	
		15.0	55.6	
		15.3	56.7	
		15.7	57.9	
		16.0	59.2	
		16.3	60.4	
		16.7	61.7	
		17.0	63.0	
		17.4	64.3	
		17.7	65.7	
		18.1	67.1	
		18.5	68.5	
		18.9	69.9	
		19.3	71.4	
		19.7	72.9	
		20.1	74.4	
		20.5	76.0	
		21.0	77.6	
		21.4	79.2	
		21.8	80.9	
		22.3	82.6	

FATIGUE CRACK GROWTH

a0= { } in
af= { } in

	1010.000	cycles	40	years
ΔN	25.250	cycles/year		
Transient	Insurge6			

Year of Operation	a (in.)	Position 10 Kmin KI(a) (ksi√in)	Kmax KI(a) (ksi√in)	Δa (in.)
		11.0	39.4	
		11.2	40.2	
		11.5	41.0	
		11.7	41.9	
		11.9	42.8	
		12.2	43.7	
		12.5	44.6	
		12.7	45.5	
		13.0	46.5	
		13.3	47.5	
		13.5	48.5	
		13.8	49.5	
		14.1	50.6	
		14.4	51.6	
		14.7	52.7	
		15.0	53.9	
		15.4	55.0	
		15.7	56.2	
		16.0	57.4	
		16.4	58.6	
		16.7	59.8	
		17.1	61.1	
		17.4	62.4	
		17.8	63.7	
		18.2	65.0	
		18.5	66.4	
		18.9	67.8	
		19.3	69.2	
		19.7	70.7	
		20.2	72.1	
		20.6	73.7	
		21.0	75.2	
		21.4	76.8	
		21.9	78.4	
		22.4	80.0	

FATIGUE CRACK GROWTH

a0= { } in
af= { } in
320.000 cycles 40 years
ΔN 8.000 cycles/year
Transient Insurge7

Year of Operation	a (in.)	Position 10 Kmin KI(a) (ksi√in)	Kmax KI(a) (ksi√in)	Δa (in.)
		22.3	51.8	
		22.7	52.9	
		23.2	54.0	
		23.7	55.1	
		24.2	56.3	
		24.7	57.5	
		25.2	58.7	
		25.7	59.9	
		26.3	61.2	
		26.8	62.5	
		27.4	63.8	
		28.0	65.2	
		28.6	66.6	
		29.2	68.0	
		29.8	69.4	
		30.5	70.9	
		31.1	72.4	
		31.8	73.9	
		32.4	75.5	
		33.1	77.1	
		33.8	78.7	
		34.5	80.4	
		35.3	82.1	
		36.0	83.8	
		36.8	85.6	
		37.5	87.4	
		38.3	89.2	
		39.1	91.1	
		40.0	93.0	
		40.8	95.0	
		41.6	97.0	
		42.5	99.0	
		43.4	101.1	
		44.3	103.2	
		45.2	105.3	

FATIGUE CRACK GROWTH

a0= { } in
af= { } in
60.000 cycles 40 years
ΔN 1.500 cycles/year
Transient Insurge8

Year of Operation	a (in.)	Position 10 Kmin KI(a) (ksi√in)	Kmax KI(a) (ksi√in)	Δa (in.)
		11.0	37.8	
		11.3	38.6	
		11.5	39.4	
		11.7	40.3	
		12.0	41.1	
		12.2	42.0	
		12.5	42.9	
		12.8	43.8	
		13.0	44.7	
		13.3	45.6	
		13.6	46.6	
		13.9	47.6	
		14.2	48.6	
		14.5	49.7	
		14.8	50.7	
		15.1	51.8	
		15.4	52.9	
		15.7	54.0	
		16.1	55.1	
		16.4	56.3	
		16.8	57.5	
		17.1	58.7	
		17.5	60.0	
		17.9	61.2	
		18.2	62.5	
		18.6	63.8	
		19.0	65.2	
		19.4	66.5	
		19.8	67.9	
		20.2	69.4	
		20.7	70.8	
		21.1	72.3	
		21.5	73.8	
		22.0	75.4	
		22.4	76.9	

FATIGUE CRACK GROWTH

a0= { } in
af= { } in
1210.000 cycles 40 years
ΔN 30.250 cycles/year
Transient Insurge9

Year of Operation	a (in.)	Position 10 Kmin KI(a) (ksi√in)	Kmax KI(a) (ksi√in)	Δa (in.)
		11.0	36.6	
		11.3	37.3	
		11.5	38.1	
		11.7	38.9	
		12.0	39.7	
		12.2	40.6	
		12.5	41.4	
		12.8	42.3	
		13.0	43.2	
		13.3	44.1	
		13.6	45.0	
		13.9	46.0	
		14.2	47.0	
		14.5	48.0	
		14.8	49.0	
		15.1	50.0	
		15.4	51.1	
		15.8	52.2	
		16.1	53.3	
		16.4	54.4	
		16.8	55.6	
		17.1	56.7	
		17.5	57.9	
		17.9	59.2	
		18.2	60.4	
		18.6	61.7	
		19.0	63.0	
		19.4	64.3	
		19.8	65.6	
		20.2	67.0	
		20.7	68.4	
		21.1	69.9	
		21.5	71.3	
		22.0	72.8	
		22.4	74.3	

FATIGUE CRACK GROWTH

a0= { } in
af= { } in

170.000 cycles 40 years
ΔN 4.250 cycles/year
Transient Insurge10

Year of Operation	a (in.)	Position 10 Kmin KI(a) (ksi√in)	Kmax KI(a) (ksi√in)	Δa (in.)
		22.2	47.9	
		22.7	48.9	
		23.2	50.0	
		23.7	51.0	
		24.2	52.1	
		24.7	53.2	
		25.2	54.3	
		25.7	55.4	
		26.3	56.6	
		26.8	57.8	
		27.4	59.0	
		28.0	60.3	
		28.6	61.6	
		29.2	62.9	
		29.8	64.2	
		30.4	65.6	
		31.1	67.0	
		31.7	68.4	
		32.4	69.8	
		33.1	71.3	
		33.8	72.8	
		34.5	74.4	
		35.2	75.9	
		36.0	77.5	
		36.7	79.2	
		37.5	80.8	
		38.3	82.5	
		39.1	84.3	
		39.9	86.0	
		40.8	87.8	
		41.6	89.7	
		42.5	91.6	
		43.4	93.5	
		44.3	95.4	
		45.2	97.4	

FATIGUE CRACK GROWTH

a0= { } in
af= { } in

1910.000 cycles 40 years
ΔN 47.750 cycles/year
Transient Insurge11

Year of Operation	a (in.)	Position 10 Kmin KI(a) (ksi√in)	Kmax KI(a) (ksi√in)	Δa (in.)
		22.1	45.8	
		22.6	46.7	
		23.1	47.7	
		23.6	48.7	
		24.1	49.7	
		24.6	50.8	
		25.1	51.8	
		25.6	52.9	
		26.2	54.0	
		26.7	55.2	
		27.3	56.4	
		27.9	57.6	
		28.5	58.8	
		29.1	60.0	
		29.7	61.3	
		30.3	62.6	
		31.0	63.9	
		31.6	65.3	
		32.3	66.7	
		33.0	68.1	
		33.7	69.5	
		34.4	71.0	
		35.1	72.5	
		35.8	74.0	
		36.6	75.6	
		37.4	77.2	
		38.1	78.8	
		38.9	80.5	
		39.8	82.1	
		40.6	83.9	
		41.4	85.6	
		42.3	87.4	
		43.2	89.2	
		44.1	91.1	
		45.0	93.0	

FATIGUE CRACK GROWTH

a0= { } in
af= { } in

350.000 cycles 40 years
ΔN 8.750 cycles/year
Transient Insurge12

Year of Operation	a (in.)	Position 10 Kmin KI(a) (ksi√in)	Kmax KI(a) (ksi√in)	Δa (in.)
		11.1	31.4	
		11.4	32.1	
		11.6	32.7	
		11.8	33.4	
		12.1	34.1	
		12.4	34.8	
		12.6	35.6	
		12.9	36.3	
		13.1	37.1	
		13.4	37.9	
		13.7	38.7	
		14.0	39.5	
		14.3	40.3	
		14.6	41.2	
		14.9	42.1	
		15.2	43.0	
		15.6	43.9	
		15.9	44.8	
		16.2	45.8	
		16.6	46.7	
		16.9	47.7	
		17.3	48.7	
		17.6	49.8	
		18.0	50.8	
		18.4	51.9	
		18.8	53.0	
		19.2	54.1	
		19.6	55.2	
		20.0	56.4	
		20.4	57.6	
		20.8	58.8	
		21.3	60.0	
		21.7	61.2	
		22.2	62.5	
		22.6	63.8	

FATIGUE CRACK GROWTH

a0= { } in
af= { } in
3360.000 cycles 40 years
ΔN 84.000 cycles/year
Transient Insurge13

Year of Operation	a (in.)	Position 10 Kmin KI(a) (ksi√in)	Kmax KI(a) (ksi√in)	Δa (in.)
		22.1	34.4	
		22.5	35.1	
		23.0	35.9	
		23.5	36.6	
		24.0	37.4	
		24.5	38.2	
		25.0	39.0	
		25.5	39.8	
		26.1	40.6	
		26.6	41.5	
		27.2	42.4	
		27.8	43.3	
		28.4	44.2	
		29.0	45.2	
		29.6	46.1	
		30.2	47.1	
		30.9	48.1	
		31.5	49.1	
		32.2	50.2	
		32.9	51.2	
		33.6	52.3	
		34.3	53.4	
		35.0	54.5	
		35.7	55.7	
		36.5	56.8	
		37.2	58.0	
		38.0	59.3	
		38.8	60.5	
		39.6	61.8	
		40.5	63.1	
		41.3	64.4	
		42.2	65.7	
		43.1	67.1	
		44.0	68.5	
		44.9	70.0	

FATIGUE CRACK GROWTH

a0= { } in
af= { } in
820.000 cycles 40 years
ΔN 20.500 cycles/year
Transient Insurge14

Year of Operation	a (in.)	Position 10 Kmin KI(a) (ksi√in)	Kmax KI(a) (ksi√in)	Δa (in.)
		11.2	21.6	
		11.4	22.1	
		11.7	22.5	
		11.9	23.0	
		12.1	23.5	
		12.4	24.0	
		12.7	24.5	
		12.9	25.0	
		13.2	25.5	
		13.5	26.1	
		13.8	26.6	
		14.1	27.2	
		14.4	27.8	
		14.7	28.3	
		15.0	28.9	
		15.3	29.6	
		15.6	30.2	
		16.0	30.8	
		16.3	31.5	
		16.6	32.1	
		17.0	32.8	
		17.3	33.5	
		17.7	34.2	
		18.1	34.9	
		18.5	35.7	
		18.9	36.4	
		19.2	37.2	
		19.7	38.0	
		20.1	38.8	
		20.5	39.6	
		20.9	40.4	
		21.4	41.3	
		21.8	42.1	
		22.3	43.0	
		22.7	43.9	

Table E-2: Downhill Detailed Crack Growth

FATIGUE CRACK GROWTH

a0= { } in
af= { } in
500.000 cycles 40 years

ΔN = 12.500 cycles/year
Transient 1B

Year of Operation	a (in.)	Position 15 Kmin KI(a) (ksi√in)	Kmax KI(a) (ksi√in)	Δa (in.)
1		0.0	15.7	
2		0.0	15.8	
3		0.1	16.0	
4		0.1	16.2	
5		0.1	16.3	
6		0.1	16.5	
7		0.1	16.7	
8		0.1	16.8	
9		0.1	17.0	
10		0.1	17.2	
11		0.1	17.4	
12		0.1	17.5	
13		0.1	17.7	
14		0.1	17.9	
15		0.1	18.1	
16		0.1	18.3	
17		0.1	18.5	
18		0.1	18.7	
19		0.1	18.9	
20		0.1	19.1	
21		0.1	19.3	
22		0.1	19.5	
23		0.1	19.8	
24		0.1	20.0	
25		0.1	20.2	
26		0.1	20.4	
27		0.1	20.7	
28		0.1	20.9	
29		0.1	21.1	
30		0.1	21.4	
31		0.1	21.6	
32		0.1	21.9	
33		0.1	22.1	
34		0.1	22.4	
35		0.1	22.7	
36		0.1	22.9	
37		0.1	23.2	
38		0.1	23.5	
39		0.1	23.7	
40		0.1	24.0	

FATIGUE CRACK GROWTH

a0= { } in
af= { } in
500.000 cycles 40 years

ΔN = 12.500 cycles/year
Transient 2B

Year of Operation	a (in.)	Position 15 Kmin KI(a) (ksi√in)	Kmax KI(a) (ksi√in)	Δa (in.)
1		4.2	16.1	
2		4.2	16.3	
3		4.3	16.4	
4		4.3	16.6	
5		4.4	16.8	
6		4.4	16.9	
7		4.4	17.1	
8		4.5	17.3	
9		4.5	17.5	
10		4.6	17.6	
11		4.6	17.8	
12		4.7	18.0	
13		4.7	18.2	
14		4.8	18.4	
15		4.8	18.6	
16		4.9	18.8	
17		4.9	19.0	
18		5.0	19.2	
19		5.0	19.4	
20		5.1	19.6	
21		5.2	19.8	
22		5.2	20.1	
23		5.3	20.3	
24		5.3	20.5	
25		5.4	20.7	
26		5.4	21.0	
27		5.5	21.2	
28		5.6	21.5	
29		5.6	21.7	
30		5.7	22.0	
31		5.8	22.2	
32		5.8	22.5	
33		5.9	22.7	
34		6.0	23.0	
35		6.0	23.3	
36		6.1	23.6	
37		6.2	23.8	
38		6.3	24.1	
39		6.3	24.4	
40		6.4	24.7	

FATIGUE CRACK GROWTH

a0= { } in
af= { } in
15000.000 cycles 40 years

ΔN = 375.000 cycles/year
Transient PL

Year of Operation	a (in.)	Position 15 Kmin KI(a) (ksi√in)	Kmax KI(a) (ksi√in)	Δa (in.)
1		15.6	17.2	
2		15.7	17.3	
3		15.9	17.5	
4		16.0	17.7	
5		16.2	17.9	
6		16.4	18.0	
7		16.5	18.2	
8		16.7	18.4	
9		16.9	18.6	
10		17.0	18.8	
11		17.2	19.0	
12		17.4	19.2	
13		17.6	19.4	
14		17.8	19.6	
15		18.0	19.8	
16		18.1	20.0	
17		18.3	20.2	
18		18.5	20.5	
19		18.7	20.7	
20		19.0	20.9	
21		19.2	21.2	
22		19.4	21.4	
23		19.6	21.6	
24		19.8	21.9	
25		20.0	22.1	
26		20.3	22.4	
27		20.5	22.6	
28		20.7	22.9	
29		21.0	23.1	
30		21.2	23.4	
31		21.5	23.7	
32		21.7	24.0	
33		22.0	24.2	
34		22.2	24.5	
35		22.5	24.8	
36		22.7	25.1	
37		23.0	25.4	
38		23.3	25.7	
39		23.5	26.0	
40		23.8	26.3	

FATIGUE CRACK GROWTH

a0= { } in
af= { } in
15000.000 cycles 40 years

ΔN = 375.000 cycles/year
Transient PU

Year of Operation	a (in.)	Position 15 Kmin KI(a) (ksi√in)	Kmax KI(a) (ksi√in)	Δa (in.)
1		15.4	17.4	
2		15.5	17.6	
3		15.7	17.8	
4		15.9	18.0	
5		16.0	18.1	
6		16.2	18.3	
7		16.3	18.5	
8		16.5	18.7	
9		16.7	18.9	
10		16.9	19.1	
11		17.0	19.3	
12		17.2	19.5	
13		17.4	19.7	
14		17.6	19.9	
15		17.8	20.1	
16		18.0	20.3	
17		18.1	20.6	
18		18.3	20.8	
19		18.5	21.0	
20		18.7	21.2	
21		19.0	21.5	
22		19.2	21.7	
23		19.4	21.9	
24		19.6	22.2	
25		19.8	22.4	
26		20.0	22.7	
27		20.3	23.0	
28		20.5	23.2	
29		20.7	23.5	
30		21.0	23.8	
31		21.2	24.0	
32		21.5	24.3	
33		21.7	24.6	
34		22.0	24.9	
35		22.2	25.2	
36		22.5	25.5	
37		22.8	25.8	
38		23.0	26.1	
39		23.3	26.4	
40		23.6	26.7	

FATIGUE CRACK GROWTH

a0= { } in
af= { } in
320.000 cycles 40 years

ΔN = 8.000 cycles/year
Transient LeakTest

Year of Operation	a (in.)	Position 15 Kmin KI(a) (ksi√in)	Kmax KI(a) (ksi√in)	Δa (in.)
1		3.2	18.5	
2		3.2	18.7	
3		3.3	18.9	
4		3.3	19.1	
5		3.3	19.3	
6		3.4	19.5	
7		3.4	19.7	
8		3.4	19.9	
9		3.5	20.1	
10		3.5	20.3	
11		3.6	20.5	
12		3.6	20.7	
13		3.6	21.0	
14		3.7	21.2	
15		3.7	21.4	
16		3.8	21.6	
17		3.8	21.9	
18		3.8	22.1	
19		3.9	22.3	
20		3.9	22.6	
21		4.0	22.8	
22		4.0	23.1	
23		4.0	23.4	
24		4.1	23.6	
25		4.1	23.9	
26		4.2	24.2	
27		4.2	24.4	
28		4.3	24.7	
29		4.3	25.0	
30		4.4	25.3	
31		4.4	25.6	
32		4.5	25.9	
33		4.5	26.2	
34		4.6	26.5	
35		4.6	26.8	
36		4.7	27.1	
37		4.8	27.4	
38		4.8	27.7	
39		4.9	28.1	
40		4.9	28.4	

FATIGUE CRACK GROWTH

a0= { } in
af= { } in
480.000 cycles 40 years

ΔN = 12.000 cycles/year
Transient LLA

Year of Operation	a (in.)	Position 15 Kmin KI(a) (ksi√in)	Kmax KI(a) (ksi√in)	Δa (in.)
1		12.0	16.7	
2		12.1	16.8	
3		12.2	17.0	
4		12.4	17.2	
5		12.5	17.3	
6		12.6	17.5	
7		12.7	17.7	
8		12.9	17.9	
9		13.0	18.1	
10		13.1	18.2	
11		13.3	18.4	
12		13.4	18.6	
13		13.6	18.8	
14		13.7	19.0	
15		13.8	19.2	
16		14.0	19.4	
17		14.1	19.6	
18		14.3	19.9	
19		14.5	20.1	
20		14.6	20.3	
21		14.8	20.5	
22		14.9	20.7	
23		15.1	21.0	
24		15.3	21.2	
25		15.4	21.5	
26		15.6	21.7	
27		15.8	21.9	
28		16.0	22.2	
29		16.2	22.5	
30		16.4	22.7	
31		16.5	23.0	
32		16.7	23.3	
33		16.9	23.5	
34		17.1	23.8	
35		17.3	24.1	
36		17.5	24.4	
37		17.7	24.6	
38		17.9	24.9	
39		18.2	25.2	
40		18.4	25.5	

CCNPP-1 PZR Heater Sleeve As-Left J-Groove Weld Flaw Evaluation for IDTB Repair

FATIGUE CRACK GROWTH

a0= { } in
af= { } in
60.000 cycles 40 years

ΔN = 1.500 cycles/year
Transient Insurge1

Year of Operation	a (in.)	Position 15 Kmin KI(a) (ksi√in)	Kmax KI(a) (ksi√in)	Δa (in.)
1		15.9	46.6	
2		16.1	47.1	
3		16.3	47.6	
4		16.4	48.1	
5		16.6	48.5	
6		16.8	49.0	
7		16.9	49.5	
8		17.1	50.0	
9		17.3	50.6	
10		17.5	51.1	
11		17.7	51.6	
12		17.8	52.2	
13		18.0	52.7	
14		18.2	53.3	
15		18.4	53.9	
16		18.6	54.4	
17		18.8	55.0	
18		19.0	55.6	
19		19.2	56.2	
20		19.4	56.8	
21		19.7	57.5	
22		19.9	58.1	
23		20.1	58.8	
24		20.3	59.4	
25		20.5	60.1	
26		20.8	60.8	
27		21.0	61.5	
28		21.3	62.2	
29		21.5	62.9	
30		21.8	63.6	
31		22.0	64.4	
32		22.3	65.1	
33		22.5	65.9	
34		22.8	66.7	
35		23.1	67.4	
36		23.3	68.2	
37		23.6	69.0	
38		23.9	69.8	
39		24.2	70.6	
40		24.4	71.4	

FATIGUE CRACK GROWTH

a0= { } in
af= { } in
70.000 cycles 40 years

ΔN = 1.750 cycles/year
Transient Insurge2

Year of Operation	a (in.)	Position 15 Kmin KI(a) (ksi√in)	Kmax KI(a) (ksi√in)	Δa (in.)
1		1.9	27.3	
2		1.9	27.5	
3		2.0	27.8	
4		2.0	28.1	
5		2.0	28.4	
6		2.0	28.7	
7		2.0	29.0	
8		2.1	29.3	
9		2.1	29.6	
10		2.1	29.9	
11		2.1	30.2	
12		2.1	30.5	
13		2.2	30.8	
14		2.2	31.1	
15		2.2	31.5	
16		2.2	31.8	
17		2.3	32.2	
18		2.3	32.5	
19		2.3	32.9	
20		2.3	33.2	
21		2.4	33.6	
22		2.4	34.0	
23		2.4	34.3	
24		2.4	34.7	
25		2.5	35.1	
26		2.5	35.5	
27		2.5	35.9	
28		2.6	36.3	
29		2.6	36.8	
30		2.6	37.2	
31		2.6	37.6	
32		2.7	38.1	
33		2.7	38.5	
34		2.7	39.0	
35		2.8	39.4	
36		2.8	39.9	
37		2.8	40.3	
38		2.9	40.8	
39		2.9	41.3	
40		2.9	41.8	

FATIGUE CRACK GROWTH

a0= { } in
af= { } in
130.000 cycles 40 years

ΔN = 3.250 cycles/year
Transient Insurge3

Year of Operation	a (in.)	Position 15 Kmin KI(a) (ksi√in)	Kmax KI(a) (ksi√in)	Δa (in.)
1		15.9	42.6	
2		16.1	43.0	
3		16.2	43.5	
4		16.4	43.9	
5		16.5	44.3	
6		16.7	44.8	
7		16.9	45.2	
8		17.1	45.7	
9		17.2	46.2	
10		17.4	46.7	
11		17.6	47.2	
12		17.8	47.6	
13		18.0	48.2	
14		18.2	48.7	
15		18.4	49.2	
16		18.6	49.7	
17		18.8	50.3	
18		19.0	50.8	
19		19.2	51.4	
20		19.4	51.9	
21		19.6	52.5	
22		19.8	53.1	
23		20.0	53.7	
24		20.3	54.3	
25		20.5	54.9	
26		20.7	55.5	
27		21.0	56.1	
28		21.2	56.8	
29		21.4	57.4	
30		21.7	58.1	
31		21.9	58.8	
32		22.2	59.5	
33		22.5	60.2	
34		22.7	60.9	
35		23.0	61.6	
36		23.3	62.3	
37		23.5	63.0	
38		23.8	63.8	
39		24.1	64.5	
40		24.4	65.3	

FATIGUE CRACK GROWTH

a0= in
af= in
530.000 cycles 40 years

ΔN = 13.250 cycles/year
Transient Insurge4

Year of Operation	a (in.)	Position 15 Kmin KI(a) (ksi√in)	Kmax KI(a) (ksi√in)	Δa (in.)
1		1.9	25.4	
2		1.9	25.6	
3		2.0	25.9	
4		2.0	26.1	
5		2.0	26.4	
6		2.0	26.7	
7		2.0	27.0	
8		2.1	27.2	
9		2.1	27.5	
10		2.1	27.8	
11		2.1	28.1	
12		2.1	28.4	
13		2.2	28.7	
14		2.2	29.0	
15		2.2	29.3	
16		2.2	29.6	
17		2.3	29.9	
18		2.3	30.3	
19		2.3	30.6	
20		2.3	30.9	
21		2.4	31.3	
22		2.4	31.6	
23		2.4	32.0	
24		2.4	32.3	
25		2.5	32.7	
26		2.5	33.1	
27		2.5	33.4	
28		2.6	33.8	
29		2.6	34.2	
30		2.6	34.6	
31		2.7	35.0	
32		2.7	35.4	
33		2.7	35.8	
34		2.7	36.3	
35		2.8	36.7	
36		2.8	37.1	
37		2.8	37.5	
38		2.9	38.0	
39		2.9	38.4	
40		2.9	38.9	

FATIGUE CRACK GROWTH

a0= in
af= in
120.000 cycles 40 years

ΔN = 3.000 cycles/year
Transient Insurge5

Year of Operation	a (in.)	Position 15 Kmin KI(a) (ksi√in)	Kmax KI(a) (ksi√in)	Δa (in.)
1		1.9	24.7	
2		1.9	24.9	
3		1.9	25.2	
4		2.0	25.4	
5		2.0	25.7	
6		2.0	26.0	
7		2.0	26.2	
8		2.0	26.5	
9		2.1	26.8	
10		2.1	27.1	
11		2.1	27.3	
12		2.1	27.6	
13		2.2	27.9	
14		2.2	28.2	
15		2.2	28.5	
16		2.2	28.8	
17		2.2	29.1	
18		2.3	29.5	
19		2.3	29.8	
20		2.3	30.1	
21		2.3	30.4	
22		2.4	30.8	
23		2.4	31.1	
24		2.4	31.5	
25		2.5	31.8	
26		2.5	32.2	
27		2.5	32.5	
28		2.5	32.9	
29		2.6	33.3	
30		2.6	33.7	
31		2.6	34.1	
32		2.7	34.5	
33		2.7	34.9	
34		2.7	35.3	
35		2.8	35.7	
36		2.8	36.1	
37		2.8	36.5	
38		2.9	37.0	
39		2.9	37.4	
40		2.9	37.8	

FATIGUE CRACK GROWTH

a0= in
af= in
1010.000 cycles 40 years

ΔN = 25.250 cycles/year
Transient Insurge6

Year of Operation	a (in.)	Position 15 Kmin KI(a) (ksi√in)	Kmax KI(a) (ksi√in)	Δa (in.)
1		1.9	23.7	
2		1.9	23.9	
3		2.0	24.2	
4		2.0	24.4	
5		2.0	24.7	
6		2.0	24.9	
7		2.0	25.2	
8		2.1	25.4	
9		2.1	25.7	
10		2.1	26.0	
11		2.1	26.2	
12		2.2	26.5	
13		2.2	26.8	
14		2.2	27.1	
15		2.2	27.4	
16		2.2	27.7	
17		2.3	28.0	
18		2.3	28.3	
19		2.3	28.6	
20		2.3	28.9	
21		2.4	29.2	
22		2.4	29.5	
23		2.4	29.8	
24		2.4	30.2	
25		2.5	30.5	
26		2.5	30.9	
27		2.5	31.2	
28		2.6	31.6	
29		2.6	32.0	
30		2.6	32.3	
31		2.7	32.7	
32		2.7	33.1	
33		2.7	33.5	
34		2.7	33.9	
35		2.8	34.3	
36		2.8	34.7	
37		2.8	35.1	
38		2.9	35.5	
39		2.9	35.9	
40		2.9	36.3	

CCNPP-1 PZR Heater Sleeve As-Left J-Groove Weld Flaw Evaluation for IDTB Repair

FATIGUE CRACK GROWTH

a0= in
af= in
320.000 cycles 40 years

ΔN = 8.000 cycles/year
Transient Insurge7

Year of Operation	a (in.)	Position 15 Kmin KI(a) (ksi√in)	Kmax KI(a) (ksi√in)	Δa (in.)
1		15.9	38.1	
2		16.1	38.5	
3		16.2	38.9	
4		16.4	39.2	
5		16.6	39.6	
6		16.7	40.0	
7		16.9	40.5	
8		17.1	40.9	
9		17.3	41.3	
10		17.4	41.7	
11		17.6	42.2	
12		17.8	42.6	
13		18.0	43.1	
14		18.2	43.5	
15		18.4	44.0	
16		18.6	44.5	
17		18.8	44.9	
18		19.0	45.4	
19		19.2	45.9	
20		19.4	46.4	
21		19.6	46.9	
22		19.8	47.5	
23		20.1	48.0	
24		20.3	48.5	
25		20.5	49.1	
26		20.7	49.6	
27		21.0	50.2	
28		21.2	50.8	
29		21.5	51.4	
30		21.7	52.0	
31		22.0	52.6	
32		22.2	53.2	
33		22.5	53.8	
34		22.8	54.4	
35		23.0	55.1	
36		23.3	55.7	
37		23.6	56.4	
38		23.8	57.0	
39		24.1	57.7	
40		24.4	58.3	

FATIGUE CRACK GROWTH

a0= in
af= in
60.000 cycles 40 years

ΔN = 1.500 cycles/year
Transient Insurge8

Year of Operation	a (in.)	Position 15 Kmin KI(a) (ksi√in)	Kmax KI(a) (ksi√in)	Δa (in.)
1		1.9	22.5	
2		1.9	22.7	
3		2.0	23.0	
4		2.0	23.2	
5		2.0	23.4	
6		2.0	23.7	
7		2.0	23.9	
8		2.1	24.1	
9		2.1	24.4	
10		2.1	24.7	
11		2.1	24.9	
12		2.2	25.2	
13		2.2	25.4	
14		2.2	25.7	
15		2.2	26.0	
16		2.2	26.3	
17		2.3	26.5	
18		2.3	26.8	
19		2.3	27.1	
20		2.3	27.4	
21		2.4	27.7	
22		2.4	28.0	
23		2.4	28.4	
24		2.5	28.7	
25		2.5	29.0	
26		2.5	29.3	
27		2.5	29.7	
28		2.6	30.0	
29		2.6	30.3	
30		2.6	30.7	
31		2.7	31.1	
32		2.7	31.4	
33		2.7	31.8	
34		2.8	32.2	
35		2.8	32.5	
36		2.8	32.9	
37		2.9	33.3	
38		2.9	33.7	
39		2.9	34.1	
40		3.0	34.5	

FATIGUE CRACK GROWTH

a0= in
af= in
1210.000 cycles 40 years

ΔN = 30.250 cycles/year
Transient Insurge9

Year of Operation	a (in.)	Position 15 Kmin KI(a) (ksi√in)	Kmax KI(a) (ksi√in)	Δa (in.)
1		1.9	21.7	
2		1.9	21.9	
3		2.0	22.1	
4		2.0	22.3	
5		2.0	22.5	
6		2.0	22.8	
7		2.0	23.0	
8		2.1	23.2	
9		2.1	23.5	
10		2.1	23.7	
11		2.1	24.0	
12		2.2	24.2	
13		2.2	24.5	
14		2.2	24.7	
15		2.2	25.0	
16		2.2	25.3	
17		2.3	25.5	
18		2.3	25.8	
19		2.3	26.1	
20		2.3	26.4	
21		2.4	26.7	
22		2.4	27.0	
23		2.4	27.3	
24		2.5	27.6	
25		2.5	27.9	
26		2.5	28.2	
27		2.5	28.5	
28		2.6	28.9	
29		2.6	29.2	
30		2.6	29.5	
31		2.7	29.9	
32		2.7	30.2	
33		2.7	30.6	
34		2.8	30.9	
35		2.8	31.3	
36		2.8	31.7	
37		2.9	32.0	
38		2.9	32.4	
39		2.9	32.8	
40		3.0	33.2	

FATIGUE CRACK GROWTH

a0= in
af= in
170.000 cycles 40 years

ΔN = 4.250 cycles/year
Transient Insurge10

Year of Operation	a (in.)	Position 15 Kmin KI(a) (ksi√in)	Kmax KI(a) (ksi√in)	Δa (in.)
1		16.0	35.1	
2		16.2	35.5	
3		16.4	35.8	
4		16.5	36.2	
5		16.7	36.5	
6		16.9	36.9	
7		17.0	37.3	
8		17.2	37.7	
9		17.4	38.1	
10		17.6	38.5	
11		17.7	38.9	
12		17.9	39.3	
13		18.1	39.7	
14		18.3	40.1	
15		18.5	40.5	
16		18.7	41.0	
17		18.9	41.4	
18		19.1	41.9	
19		19.3	42.3	
20		19.5	42.8	
21		19.8	43.3	
22		20.0	43.7	
23		20.2	44.2	
24		20.4	44.7	
25		20.7	45.2	
26		20.9	45.7	
27		21.1	46.3	
28		21.4	46.8	
29		21.6	47.3	
30		21.9	47.9	
31		22.1	48.4	
32		22.4	49.0	
33		22.6	49.6	
34		22.9	50.2	
35		23.2	50.7	
36		23.4	51.3	
37		23.7	51.9	
38		24.0	52.5	
39		24.3	53.2	
40		24.6	53.8	

FATIGUE CRACK GROWTH

a0= in
af= in
1910.000 cycles 40 years

ΔN = 47.750 cycles/year
Transient Insurge11

Year of Operation	a (in.)	Position 15 Kmin KI(a) (ksi√in)	Kmax KI(a) (ksi√in)	Δa (in.)
1		16.0	33.7	
2		16.1	34.0	
3		16.3	34.3	
4		16.4	34.7	
5		16.6	35.0	
6		16.8	35.4	
7		17.0	35.8	
8		17.1	36.1	
9		17.3	36.5	
10		17.5	36.9	
11		17.7	37.3	
12		17.9	37.6	
13		18.0	38.0	
14		18.2	38.5	
15		18.4	38.9	
16		18.6	39.3	
17		18.8	39.7	
18		19.0	40.1	
19		19.2	40.6	
20		19.5	41.0	
21		19.7	41.5	
22		19.9	41.9	
23		20.1	42.4	
24		20.3	42.9	
25		20.6	43.4	
26		20.8	43.9	
27		21.0	44.4	
28		21.3	44.9	
29		21.5	45.4	
30		21.8	45.9	
31		22.0	46.5	
32		22.3	47.0	
33		22.5	47.5	
34		22.8	48.1	
35		23.1	48.7	
36		23.3	49.2	
37		23.6	49.8	
38		23.9	50.4	
39		24.2	51.0	
40		24.5	51.6	

FATIGUE CRACK GROWTH

a0= in
af= in
350.000 cycles 40 years

ΔN = 8.750 cycles/year
Transient Insurge12

Year of Operation	a (in.)	Position 15 Kmin KI(a) (ksi√in)	Kmax KI(a) (ksi√in)	Δa (in.)
1		1.9	17.6	
2		2.0	17.8	
3		2.0	18.0	
4		2.0	18.1	
5		2.0	18.3	
6		2.0	18.5	
7		2.1	18.7	
8		2.1	18.9	
9		2.1	19.1	
10		2.1	19.3	
11		2.1	19.5	
12		2.2	19.7	
13		2.2	19.9	
14		2.2	20.1	
15		2.2	20.3	
16		2.3	20.5	
17		2.3	20.8	
18		2.3	21.0	
19		2.3	21.2	
20		2.4	21.4	
21		2.4	21.7	
22		2.4	21.9	
23		2.4	22.2	
24		2.5	22.4	
25		2.5	22.7	
26		2.5	22.9	
27		2.6	23.2	
28		2.6	23.5	
29		2.6	23.7	
30		2.6	24.0	
31		2.7	24.3	
32		2.7	24.6	
33		2.7	24.9	
34		2.8	25.1	
35		2.8	25.4	
36		2.8	25.7	
37		2.9	26.0	
38		2.9	26.3	
39		2.9	26.6	
40		3.0	27.0	

FATIGUE CRACK GROWTH

a0= { } in
af= { } in
3360.000 cycles 40 years

ΔN = 84.000 cycles/year
Transient Insurge13

Year of Operation	a (in.)	Position 15 Kmin KI(a) (ksi√in)	Kmax KI(a) (ksi√in)	Δa (in.)
1		16.0	25.0	
2		16.1	25.2	
3		16.3	25.5	
4		16.5	25.7	
5		16.6	26.0	
6		16.8	26.3	
7		17.0	26.5	
8		17.1	26.8	
9		17.3	27.1	
10		17.5	27.4	
11		17.7	27.7	
12		17.9	27.9	
13		18.1	28.2	
14		18.3	28.5	
15		18.4	28.9	
16		18.6	29.2	
17		18.8	29.5	
18		19.1	29.8	
19		19.3	30.1	
20		19.5	30.5	
21		19.7	30.8	
22		19.9	31.1	
23		20.1	31.5	
24		20.4	31.8	
25		20.6	32.2	
26		20.8	32.6	
27		21.1	32.9	
28		21.3	33.3	
29		21.5	33.7	
30		21.8	34.1	
31		22.1	34.5	
32		22.3	34.9	
33		22.6	35.3	
34		22.8	35.7	
35		23.1	36.1	
36		23.4	36.5	
37		23.6	37.0	
38		23.9	37.4	
39		24.2	37.8	
40		24.5	38.3	

FATIGUE CRACK GROWTH

a0= { } in
af= { } in
820.000 cycles 40 years

ΔN = 20.500 cycles/year
Transient Insurge14

Year of Operation	a (in.)	Position 15 Kmin KI(a) (ksi√in)	Kmax KI(a) (ksi√in)	Δa (in.)
1		1.9	9.9	
2		2.0	10.0	
3		2.0	10.1	
4		2.0	10.2	
5		2.0	10.3	
6		2.0	10.4	
7		2.1	10.5	
8		2.1	10.6	
9		2.1	10.8	
10		2.1	10.9	
11		2.1	11.0	
12		2.2	11.1	
13		2.2	11.2	
14		2.2	11.3	
15		2.2	11.5	
16		2.3	11.6	
17		2.3	11.7	
18		2.3	11.8	
19		2.3	12.0	
20		2.4	12.1	
21		2.4	12.2	
22		2.4	12.4	
23		2.4	12.5	
24		2.5	12.6	
25		2.5	12.8	
26		2.5	12.9	
27		2.6	13.1	
28		2.6	13.2	
29		2.6	13.4	
30		2.6	13.5	
31		2.7	13.7	
32		2.7	13.9	
33		2.7	14.0	
34		2.8	14.2	
35		2.8	14.4	
36		2.8	14.5	
37		2.9	14.7	
38		2.9	14.9	
39		2.9	15.0	
40		3.0	15.2	